the ECG features presented here to locate subjects in wide populations, such as health examinations, who are at risk.

Acknowledgments

The authors thank Kahaku Emoto, Seiichi Fujisaki, and Tatsumi Uchiyama (GE Yokokawa Medical System Co) for their technical assistance.

Disclosures

No conflicts to disclose.

References

1. Brugada P, Brugada J. Right bundle branch block, persistent ST segment elevation and sudden cardiac death: A distinct clinical and electrocardiographic syndrome: A multicenter report. *J Am Coll Cardiol* 1992; **20:** 1391–1396.
2. Antzelevitch C, Brugada P, Borggrefe M, Brugada J, Brugada R, Corrado D, et al. Brugada syndrome: Report of the second consensus conference: Endorsed by the heart rhythm society and the european heart rhythm association. *Circulation* 2005; **111:** 659–670.
3. Miyasaka Y, Tsuji H, Yamada K, Tokunaga S, Saito D, Imuro Y, et al. Prevalence and mortality of the Brugada-type electrocardiogram in one city in japan. *J Am Coll Cardiol* 2001; **38:** 771–774.
4. Matsuo K, Akahoshi M, Nakashima E, Suyama A, Seto S, Hayano M, et al. The prevalence, incidence and prognostic value of the Brugada-type electrocardiogram: A population-based study of four decades. *J Am Coll Cardiol* 2001; **38:** 765–770.
5. Brugada J, Brugada R, Antzelevitch C, Towbin J, Nademanee K, Brugada P. Long-term follow-up of individuals with the electrocardiographic pattern of right bundle-branch block and ST-segment elevation in precordial leads V1 to V3. *Circulation* 2002; **105:** 73–78.
6. Priori SG, Napolitano C, Gasparini M, Pappone C, Della Bella P, Giordano U, et al. Natural history of Brugada syndrome: Insights for risk stratification and management. *Circulation* 2002; **105:** 1342–1347.
7. Eckardt L, Probst V, Smits JP, Bahr ES, Wolpert C, Schimpf R, et al. Long-term prognosis of individuals with right precordial ST-segment-elevation brugada syndrome. *Circulation* 2005; **111:** 257–263.
8. Brugada P, Brugada R, Brugada J. Should patients with an asymptomatic Brugada electrocardiogram undergo pharmacological and electrophysiological testing? *Circulation* 2005; **112:** 279–292; discussion 279–292.
9. Priori SG, Napolitano C. Should patients with an asymptomatic Brugada electrocardiogram undergo pharmacological and electrophysiological testing? *Circulation* 2005; **112:** 279–292; discussion 279–292.
10. Chen Q, Kirsch GE, Zhang D, Brugada R, Brugada J, Brugada P, et al. Genetic basis and molecular mechanism for idiopathic ventricular fibrillation. *Nature* 1998; **392:** 293–296.
11. Makiyama T, Akao M, Shizuta S, Doi T, Nishiyama K, Oka Y, et al. A novel scn5a gain-of-function mutation M1875T associated with familial atrial fibrillation. *J Am Coll Cardiol* 2008; **52:** 1326–1334.
12. Kawamura M, Ozawa T, Yao T, Ashihara T, Sugimoto Y, Yagi T, et al. Dynamic change in ST-segment and spontaneous occurrence of ventricular fibrillation in Brugada syndrome with a novel nonsense mutation in the SCN5A gene during long-term follow-up. *Circ J* 2009; **73:** 584–588.
13. Yan GX, Antzelevitch C. Cellular basis for the Brugada syndrome and other mechanisms of arrhythmogenesis associated with ST-segment elevation. *Circulation* 1999; **100:** 1660–1666.
14. Nagase S, Kusano KF, Morita H, Nishii N, Banba K, Watanabe A, et al. Longer repolarization in the epicardium at the right ventricular outflow tract causes type 1 electrocardiogram in patients with Brugada syndrome. *J Am Coll Cardiol* 2008; **51:** 1154–1161.
15. Ashino S, Watanabe I, Kofune M, Nagashima K, Ohkubo K, Okumura Y, et al. Abnormal action potential duration restitution property in the right ventricular outflow tract in Brugada syndrome. *Circ J* 2010; **74:** 664–670.
16. Kanda M, Shimizu W, Matsuo K, Nagaya N, Taguchi A, Suyama K, et al. Electrophysiologic characteristics and implications of induced ventricular fibrillation in symptomatic patients with Brugada syndrome. *J Am Coll Cardiol* 2002; **39:** 1799–1805.
17. Morita H, Kusano-Fukushima K, Nagase S, Fujimoto Y, Hisamatsu K, Fujio H, et al. Atrial fibrillation and atrial vulnerability in patients with Brugada syndrome. *J Am Coll Cardiol* 2002; **40:** 1437–1444.
18. Kusano KF, Taniyama M, Nakamura K, Miura D, Banba K, Nagase S, et al. Atrial fibrillation in patients with Brugada syndrome relationships of gene mutation, electrophysiology, and clinical backgrounds. *J Am Coll Cardiol* 2008; **51:** 1169–1175.
19. Yamada T, Watanabe I, Okumura Y, Takagi Y, Okubo K, Hashimoto K, et al. Atrial electrophysiological abnormality in patients with Brugada syndrome assessed by P-wave signal-averaged ECG and programmed atrial stimulation. *Circ J* 2006; **70:** 1574–1579.
20. Hayashi H, Sumiyoshi M, Yasuda M, Komatsu K, Sekita G, Kawano Y, et al. Prevalence of the Brugada-type electrocardiogram and incidence of Brugada syndrome in patients with sick sinus syndrome. *Circ J* 2010; **74:** 271–277.
21. Brugada J, Brugada R, Brugada P. Right bundle-branch block and ST-segment elevation in leads V1 through V3: A marker for sudden death in patients without demonstrable structural heart disease. *Circulation* 1998; **97:** 457–460.

Supplemental Files

Supplemental File 1

Figure S1. 12-lead ECG of a 49-year-old man who was diagnosed with Brugada syndrome.

Figure S2. 12-lead ECG of a 55-year-old man who was undiagnosed with Brugada syndrome.

Table S1. Comparison of ECG Variables Between Patients With and Without ICD Intervention in the BS Diagnosis Group

Please find supplementary file(s);
http://dx.doi.org/10.1253/circj.CJ-10-0903

Reciprocal Control of hERG Stability by Hsp70 and Hsc70 With Implication for Restoration of LQT2 Mutant Stability

Peili Li, Haruaki Ninomiya, Yasutaka Kurata, Masaru Kato, Junichiro Miake, Yasutaka Yamamoto, Osamu Igawa, Akira Nakai, Katsumi Higaki, Futoshi Toyoda, Jie Wu, Minoru Horie, Hiroshi Matsuura, Akio Yoshida, Yasuaki Shirayoshi, Masayasu Hiraoka, Ichiro Hisatome

Rationale: **The human ether-a-go-go–related gene (hERG) encodes the α subunit of the potassium current I_{Kr}. It is highly expressed in cardiomyocytes and its mutations cause long QT syndrome type 2. Heat shock protein (Hsp)70 is known to promote maturation of hERG. Hsp70 and heat shock cognate (Hsc70) 70 has been suggested to play a similar function. However, Hsc70 has recently been reported to counteract Hsp70.**

Objective: **We investigated whether Hsc70 counteracts Hsp70 in the control of wild-type and mutant hERG stability.**

Methods and Results: **Coexpression of Hsp70 with hERG in HEK293 cells suppressed hERG ubiquitination and increased the levels of both immature and mature forms of hERG. Immunocytochemistry revealed increased levels of hERG in the endoplasmic reticulum and on the cell surface. Electrophysiological studies showed increased I_{Kr}. All these effects of Hsp70 were abolished by Hsc70 coexpression. Heat shock treatment of HL-1 mouse cardiomyocytes induced endogenous Hsp70, switched mouse ERG associated with Hsc70 to Hsp70, increased I_{Kr}, and shortened action potential duration. Channels with disease-causing missense mutations in intracellular domains had a higher binding capacity to Hsc70 than wild-type channels and channels with mutations in the pore region. Knockdown of Hsc70 by small interfering RNA or heat shock prevented degradation of mutant hERG proteins with mutations in intracellular domains.**

Conclusions: **These results indicate reciprocal control of hERG stability by Hsp70 and Hsc70. Hsc70 is a potential target in the treatment of LQT2 resulting from missense hERG mutations. (*Circ Res*. 2011;108:458-468.)**

Key Words: hERG ■ Hsp70 ■ Hsc70 ■ stabilization ■ long QT2

The human ether-a-go-go–related gene (hERG) encodes the α subunit of a rapidly activating delayed-rectifier K^+ current (I_{Kr}),[1–3] which controls the action potential duration in cardiomyocytes. Mutations in the gene cause long-QT syndrome type 2 (LQT2), a disorder that leads to life-threatening arrhythmia. To date, more than 200 naturally occurring mutations of hERG have been identified. Functional analysis of mutant proteins showed that most of them had an impairment of protein maturation and/or trafficking.[4–6] They are recognized by the quality control machinery of the endoplasmic reticulum (ER), ubiquitinated, and eventually degraded by the proteasomal degradation system.[6–8] The maturation of hERG can be evaluated by comparing the levels of the 2 forms of this protein; a core-glycosylated, immature form of 135-kDa localized in the ER, and a fully glycosylated mature form of 155 kDa localized either in the Golgi apparatus or on cell surface.[7,9]

Molecular chaperones participate in every step of hERG biogenesis, including synthesis, folding, assembly, and translocation.[8,10,11] The heat shock protein (Hsp)70 family, including stress-induced Hsp70 and constitutively expressed heat shock cognate protein (Hsc)70, interact with the core-glycosylated form of hERG.[8,12] Hsp70 increases the levels of both immature and mature forms of hERG,[8] whereas the role of Hsc70 remains unknown. In other channel proteins, such as the murine epithelial sodium channel, Hsc70 has been shown to counteract the action of Hsp70 and, thus, decreases the level of the channel protein.[13] The primary purpose of this study was to examine whether Hsc70 had a similar action on hERG. For this purpose, we investigated the effects of Hsp70 and Hsc70 on the level of

Original received July 6, 2010; revision received December 6, 2010; accepted December 13, 2010. In November 2010, the average time from submission to first decision for all original research papers submitted to *Circulation Research* was 13.2 days.

From the Department of Genetic Medicine and Regenerative Therapeutics (P.L., J.M., Y.Y., A.Y., Y.S., I.H.), Institute of Regenerative Medicine and Biofunction; Department of Biological Regulation (H.N.); Research Center for Bioscience and Technology (K.H.); Department of Cardiovascular Medicine (M.K., O.I.), Tottori University; Department of Physiology II (Y.K.), Kanazawa Medical University; Department of Biochemistry and Molecular Biology (A.N.), Yamaguchi University School of Medicine; Departments of Physiology (F.T., H.M.) and Cardiovascular Medicine (J.W., M. Horie) Shiga University of Medical Science; and Department of Cardiovascular Diseases, Tokyo Medical and Dental University (M. Hiraoka), Japan.

Correspondence to Ichiro Hisatome, Department of Genetic Medicine and Regenerative Therapeutics, 36-1, Nishimachi, Yonago, Tottori, 683-8503, Japan. E-mail hisatome@med.tottori-u.ac.jp

Circulation Research **is available at http://circres.ahajournals.org** **DOI: 10.1161/CIRCRESAHA.110.227835**

hERG proteins by biochemical and electrophysiological methods. Their effects were examined on exogenous hERG expressed in HEK293 cells as well as on endogenous proteins expressed in HL-1 cardiomyocytes. We also extended our study to examine an interaction of Hsc70 with mutant hERG proteins harboring disease-causing missense mutations.

Non-standard Abbreviations and Acronyms	
APD	action potential duration
APD_{90}	action potential duration at 90% repolarization
ER	endoplasmic reticulum
ERG	ether-a-go-go–related gene
hERG	human ether-a-go-go-related gene
HS	heat shock
Hsp70	heat shock protein 70
Hsc70	heat shock cognate protein 70
IB	immunoblot
I_{Kr}	rapidly activating delayed rectifier K^+ current
IP	immunoprecipitates
LQT2	long QT syndrome type 2
mERG	mouse ether-a-go-go-related gene
siRNA	small interfering RNA
WT	wild type

Methods

An expanded Methods section is available in the Online Data Supplement at http://circres.ahajournals.org.

HEK293 cells were cultured in DMEM (Sigma) supplemented with 10% FBS (JRH) and penicillin/streptomycin/geneticin at 37°C, 5% CO_2.[14–17] HL-1 mouse cardiomyocytes were maintained as previously described.[18] An expression construct pcDNA3/hERG-FLAG was engineered by ligating an oligonucleotide encoding a FLAG epitope to the carboxy terminus of hERG cDNA. Missense mutations were introduced into pcDNA3/ hERG-FLAG by site-directed mutagenesis. Transfection into HEK293 and HL-1 cells were performed using Lipofectamine 2000 (Invitrogen) or Nucleofector technology (Amaxa Biosystems, Gaithersburg, MD), respectively, following the protocol of the manufacturer. pEGFP was added into all the experiments of transfection to trace the transfection efficiency. HEK293 cells stably expressing hERG-FLAG were transfected with pcDNA3/ Hsc70 or Hsp70 together with pEGFP. Twenty-four hours after transfection, cells were visualized by EGFP fluorescence and hERG channel currents corresponding to I_{Kr} were measured at 37°C using whole-cell patch-clamp techniques. Procedures for the current measurement in HL-1 cells were essentially the same as described previously.[19] The membrane potential was held at −50 mV to inactivate the T-type Ca^{2+} channel current ($I_{Ca,T}$) and avoid the hyperpolarization-activated cation current (I_f) activation,[20,21] depolarized by 1-second test pulses (from −40 and +40- in 10-mV increments), then repolarized back to the holding potential; 0.4 μmol/L nisoldipine was included in the bath solution to block the L-type Ca^{2+} channel current ($I_{Ca,L}$).[20] Action potentials were also measured in the current-clamp mode, elicited at a rate of 0.5 Hz by 5-ms square current pulses of 1 nA, and sampled at 20 kHz in the absence or presence of 10 μmol/L E4031 (WAKO, Japan).

Results

Hsp70 and Hsc70 Exert Opposite Effects on the Maturation of hERG

We first examined effects of Hsp70 on hERG-FLAG expressed in HEK293 cells. As expected, hERG-FLAG gave 2 bands on the anti-FLAG immunoblot (IB), a fully glycosylated mature form of 155-kDa and an immature core-glycosylated form of 135-kDa (Figure 1A). Coexpression of Hsp70 increased the levels of both forms in a dose-dependent manner with a concomitant decrease in the ubiquitinated form of the protein. hERG was recovered in the detergent-soluble fraction, whether Hsp70 was expressed or not, suggesting that Hsp70 did not induce changes in protein solubility (Online Figure I, A). Hsp70 did not alter the level of hERG-FLAG mRNA (Online Figure I, B). Small interfering (si)RNAs targeted against Hsp70 caused marked decreases of both immature and mature forms of hERG-FLAG and also an increase in its ubiquitinated form (Figure 1B).

In contrast, coexpression of Hsc70 decreased the levels of both forms of hERG in a dose-dependent manner. The decreases were accompanied by an increase in its ubiquitinated form (Figure 1C). siRNAs targeted against Hsc70 caused a marked increase of both forms and also a decrease in its ubiquitinated form (Figure 1D). Hsc70 did not alter either solubility of hERG-FLAG or the level of its mRNA (Online Figure I, C and D). We then determined the half- life of hERG-FLAG by chase experiments (Figure 2). The half-life of the 135-kDa immature form was 9.5±3.1 hour in the control and was prolonged to 13±2.5 hours when cotransfected with Hsp70, whereas it was shortened to 6.8±2.3 hours by coexpression of Hsc70.

Next, we examined effects of Hsp70 and Hsc70 on intracellular localization of hERG-FLAG (Figure 3A). The immunoreactivity of hERG-FLAG was localized in the ER (nos. 1 to 3), the Golgi apparatus (nos. 4 to 6), and on the cell membrane (nos. 7 to 9), as evidenced by colocalization with calnexin, Golgi-GFP and GFP-Mem, respectively. Hsp70 appeared to increase the signals in all of these cellular components; and Hsc70 caused opposite effects. The changes in immunoreactivities were confirmed by a quantification analysis (Figure 3B).

The intracellular localization of hERG-FLAG was further confirmed by subcellular fractionation on the Optiprep gradient (Figure 3C). A membrane marker Na^+/K^+ ATPase was enriched in fractions 2 to 5, whereas an ER marker calnexin was enriched in nos. 10 to 15. Hsp70 increased the levels of hERG-FLAG in both fraction nos. 2 to 5 and nos. 11 to 16. Both Hsp70 and Hsc70 were enriched in fraction nos. 11 to 16, suggesting that the main site of action of these proteins was the ER.

To see whether Hsp70/Hsc70 affected the levels of functional hERG, we measured hERG channel currents in HEK293 cells stably expressing hERG-FLAG. Depolarizing pulses activated time-dependent outward currents corresponding to I_{Kr} (Figure 4A), and these currents were completely blocked by E4031 (10 μmol/L) as indicated by the disappearance of the tail currents (Online Figure II, A). The kinetics of the currents through hERG without the FLAG tag was nearly identical to those of the currents through hERG-FLAG, excluding an effect of the tag on hERG currents (Online Figure II, B). Hsp70 caused remarkable increases in both the peak and tail current amplitudes (Figure 4A through 4C). In contrast, Hsc70 reduced the peak currents during depolarization by approximately 49% and tail currents by approximately 58% (Figure 4A through 4C).

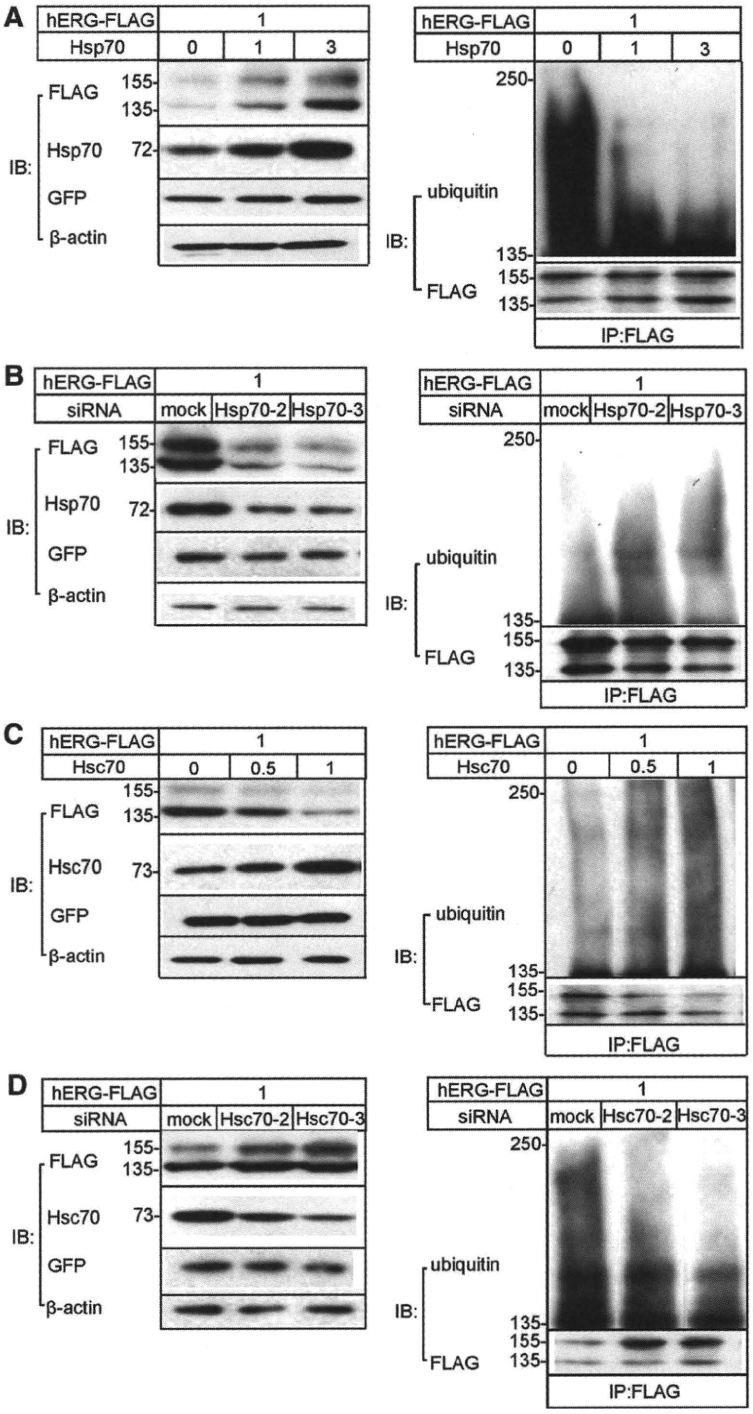

Figure 1. Effects of Hsp70 /Hsc70 on the levels of hERG-FLAG and its ubiquitination in HEK293 cells. Cells were transiently transfected with hERG-FLAG, pEGFP, and either Hsp70 **(A)** or Hsc70 **(C)**. HEK293 cells transfected with hERG-FLAG constructs were treated with either a scramble siRNA (mock) or siRNA against Hsp70 **(B)** or Hsc70 **(D)** (n=5 to 9). The amounts of plasmids (μg) are indicated in each **panel**. Shown are representative blots. Cell extracts were subjected to IB with indicated antibodies (n=4 to 11) **(left)** or anti-FLAG immunoprecipitates (IP) were subjected to IB with anti-ubiquitin or FLAG antibody (n=5 to 7) **(right)**.

Both Hsp70 and Hsc70 Associate With hERG-FLAG

To explore a biochemical basis for the opposite effects of Hsp70 and Hsc70, we examined their association with hERG by immunoprecipitation. The anti-FLAG immunoprecipitates (IPs) from hERG-expressing HEK293 cells contained endogenous Hsp70 and Hsc70 (Figure 5A). Both anti-Hsp70 and anti-Hsc70 IPs contained the 135-kDa immature form of hERG, but not the 155-kDa mature form, suggesting selective association of these chaperones with the immature form (Figure 5B). The specificity of Hsp70 and Hsc70 antibodies was confirmed by Western blotting using Hsp70 or Hsc70 recombinant proteins (Online Figure III, A).

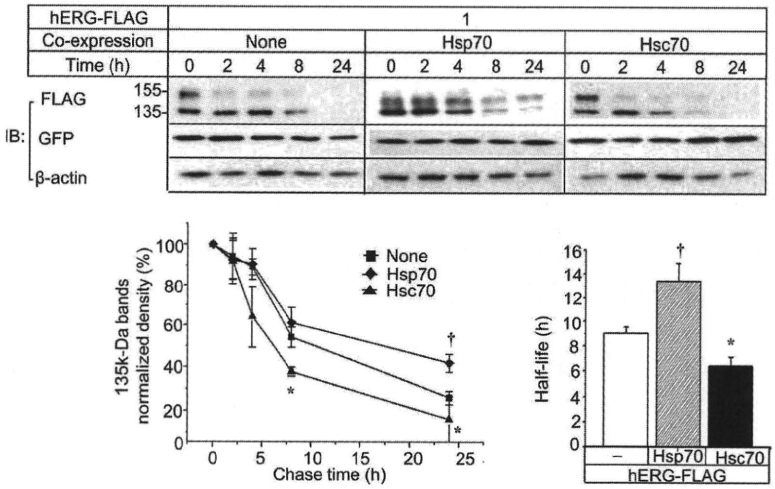

Figure 2. Degradation of hERG-FLAG proteins. HEK293 cells transiently expressing hERG-FLAG together with Hsp70 or Hsc70 were chased for the indicated time after addition of cycloheximide. Shown are the representative blot and time-dependent changes in the density of hERG-FLAG. The density of 135-kDa hERG-FLAG was normalized to the density at time 0 and β-actin. **Bar graph** shows half-life of hERG proteins. *$P<0.05$, †$P<0.01$ vs hERG-FLAG only (none) (n=6 to 7).

Coexpression of Hsp70 increased the levels of hERG-FLAG recovered by anti-FLAG. Cotransfection of Hsc70 with Hsp70 diminished the increases of hERG-FLAG in a dose-dependent manner (Figure 5C). Accordingly, the level of Hsp70 in anti-FLAG IPs was reduced by Hsc70, and this reduction was accompanied by an increase in the level of Hsc70 in the IPs (Figure 5D). These data suggested that Hsp70 and Hsc70 compete with each other in an interaction with hERG.

Regulation of Endogenous Mouse ERG and Cardiac Action Potential Duration by Hsp70 and Hsc70

To evaluate the physiological roles of Hsp70 and Hsc70 in the stability control of endogenous mouse (m)ERG, we used HL-1 mouse cardiomyocytes. In these cells, the anti-mERG antibody recognized an intense band at 155-kDa and a faint band at 135-kDa (Figure 6A). Immunoprecipitation with the anti-mERG antibody revealed an association of this protein with both Hsp70 and Hsc70 (Online Figure III, B). Hsp70 but neither Hsp90 nor Hsc70 was induced by a heat shock (HS) treatment at 42°C for 1 hour (Figure 6A), indicating selective induction of Hsp70 by HS. This increase in Hsp70 was accompanied by an apparent increase in the levels of both 135-kDa immature and 155-kDa mature forms of mERG. Under control conditions, anti-mERG IPs contained only Hsc70. After the HS, the same IPs contained Hsp70. Thus, HS-induced increase in Hsp70 switched the chaperone associated with mERG from Hsc70 to Hsp70 (Figure 6B).

siRNAs against Hsp70 were introduced into cells treated with the HS, because of the low level of Hsp70 in HL-1 cells. The siRNAs obviously decreased the level of Hsp70. The levels of both forms of mERG were also decreased compared with the levels in cells given a scrambled siRNA (Figure 6C, left). In contrast, siRNAs against Hsc70 increased the level of the Hsp70-mERG complex (Figure 6C, right). Hsp70 or Hsc70 was expressed in HL-1 cells using nucleofactor with transfection efficiency up to 90%. Hsp70 increased both forms of mERG, whereas Hsc70 diminished them (Figure 6D).

We next recorded I_{Kr} as the E4031-sensitive current in control and HS- treated HL-1 cells. The possible contamination of other voltage-dependent currents was minimized by adding 0.4μmol/L nisoldipine to bath solution to block $I_{Ca,L}$[20] and by setting a holding potential at −50mV to inactivate $I_{Ca,T}$ and to prevent activation of I_f.[20,21] Figure 7A shows whole-cell membrane currents recorded in HL-1. Depolarizing pulses activated time-dependent outward currents which increased with depolarization up to 0 mV (Control, None). The application of E4031 (10μmol/L) almost completely abolished the time-dependent outward current and the tail current (Control, E4031). E4031-sensitive current traces were obtained by digitally subtracting the current traces in the presence of E4031 from the traces in the absence ofE4031. The E4031-sensitive and -free currents have similar characteristics and current-voltage relationship, reflecting that I_{Kr} is the most prominent outward current in HL-1 cells. HS caused significant increases in both I_{Kr} peak and tail currents (Figure 7A and 7B).

Because the mERG current is responsible for repolarization of the cardiac action potential and I_{Kr} is the dominant outward current in HL-1cells,[18,22] we examined whether HS altered action potential duration (APD) in HL-1 cells. As shown in Figure 7C (a), the HS shortened APD at 90% repolarization (APD_{90}) without affecting resting membrane potentials. The APD_{90} values in control and under HS treatment were 147.6±5.6 and 63.0±5.1 ms, respectively (Figure 7C, e). In accordance with these results, Hsp70 siRNA prolonged APD_{90} as E4031 treatment, whereas Hsc70 siRNA shortened APD_{90}, regardless of the HS treatment (Figure 7C, b through d). Figure 7C (e) summarizes APD_{90} values.

Because E4031 is a specific blocker of I_{Kr}, comparing the APD_{90} to that with and without E4031 treatment (the ratio of APD_{90} E4031/APD_{90} control) clarifies the contribution of I_{Kr} to APD_{90}. As shown in Online Figure IV, HS treatment significantly increased the ratio of APD_{90} E4031/APD_{90} compared to that of control, whereas its effect was abolished by siRNA Hsp70. This indicated that HS-induced shortening of APD_{90} was attributable to an increase of I_{Kr} via activation of Hsp70. Interestingly, siRNA against Hsc70 also significantly increased the ratio of APD_{90} E4031/APD_{90} control, suggesting that APD_{90} may normally be under Hsc70 control.

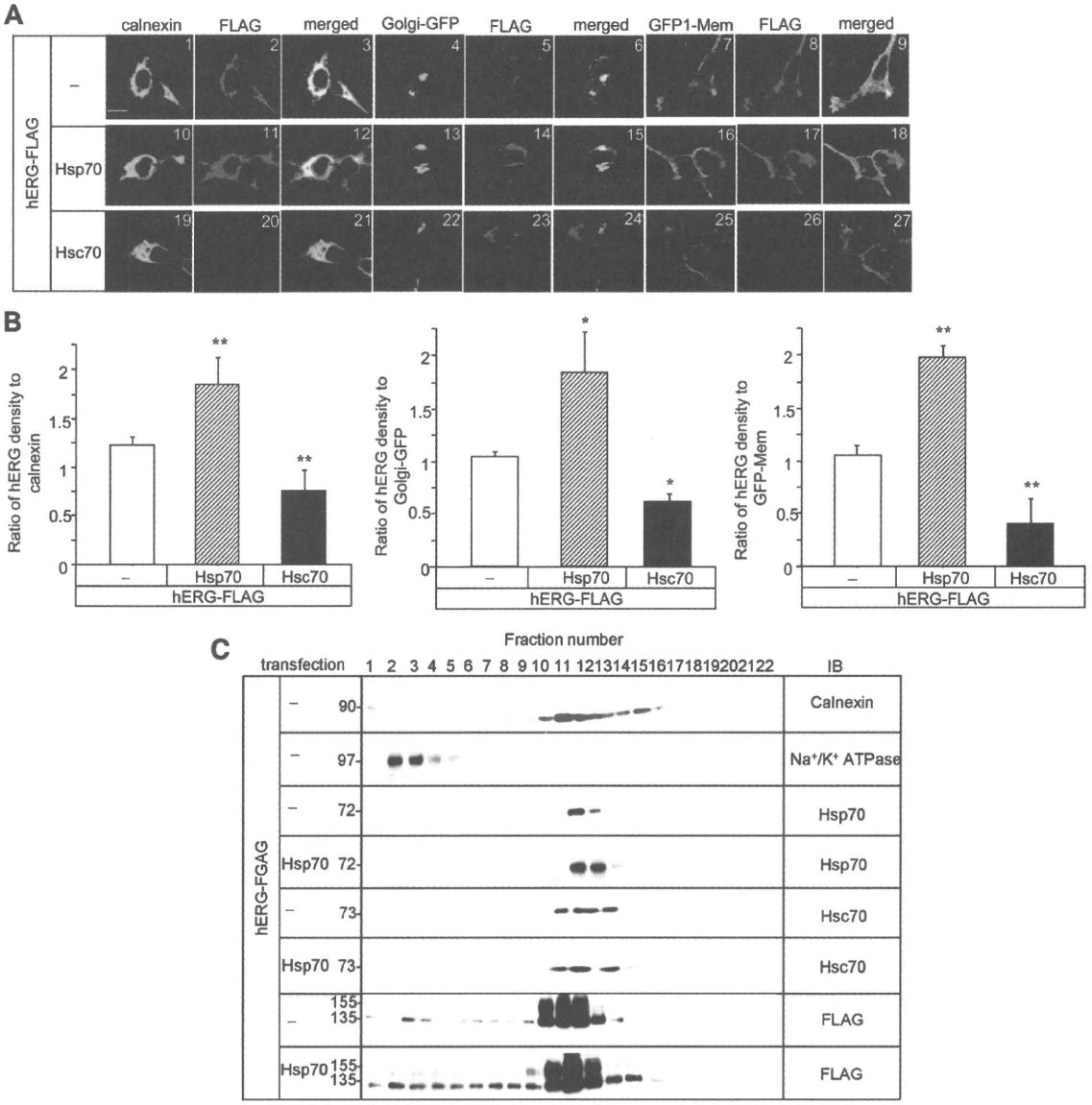

Figure 3. Intracellular localization of hERG-FLAG. A, Immunofluorescence of hERG-FLAG in HEK293 cells. Cells were transfected with hERG-FLAG together with pcDNA3 or Hsp70 or Hsc70 expression constructs. Parts of the cells were cotransfected with pAcGFP-Mem or Golgi-GFP. One set of cells was immunostained by calnexin **(green)**. All the cells were stained with anti-FLAG and Alexa Fluor 546–conjugated secondary antibody **(red)**. Shown are representative images obtained by a confocal microscope. **Bar,** 20 μm. **B,** Quantification of anti-FLAG immunoreactivity. Shown is the ratio of intensity for Alexa 546/calnexin, Golgi-GFP, or pAcGFP-Mem fluorescence. Each **column** represents the mean±SEM of 12 to 15 determinations. $^{**}P<0.01$, $^{*}P<0.05$ vs mock (none) (n=12 to 15). **C,** Cell fractionation. Whole-cell homogenates were prepared from HEK293 cells transiently expressing hERG-FLAG or with Hsp70 after 48 hours of transfection. The postnuclear supernatants were fractionated by a liner gradient of iodixanol. hERG-FLAG protein and various organelle markers were detected by IB analyses.

Stability Control of hERG Mutant Proteins by Hsp70 and Hsc70

Because mutations of hERG impair their stability, we examined binding activities of mutant hERG to Hsp70 and Hsc70. For this purpose, we engineered 10 kinds of mutant hERG proteins. The location of each missense mutation is depicted in Figure 8A (top). Figure 8A (bottom) shows representative IBs of cell lysates from HEK293 cells expressing either wild-type (WT) or various mutant hERG-FLAG. All of the mutant hERG gave only the 135-kDa band. IP experiments showed that the mutants with mutations in intracellular domains preferentially associated with Hsc70; whereas those with mutations in the pore-region preferentially associated with Hsp70.

We then examined degradation of 2 kinds of mutant proteins, P596R, a mutation located in the pore-region, and F805C, an intracellular domain mutation. Chase experiments showed that F805C and P596R had half-life of 4.3±1.5 hours and 7.4±3.7 hours (n=5 to 7, $P<0.05$), respectively. Hsc70

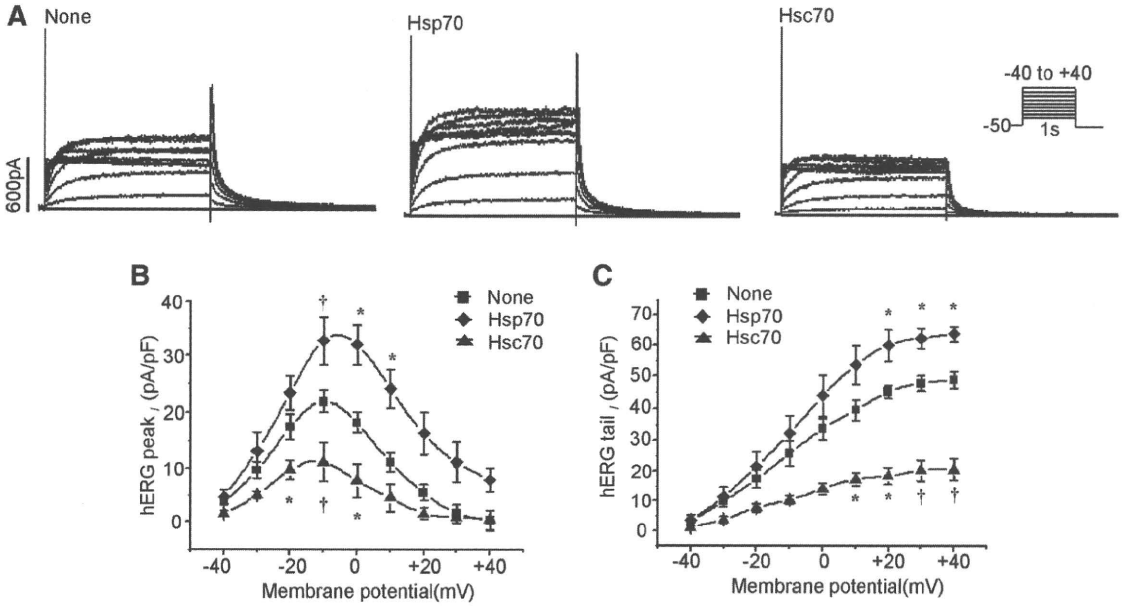

Figure 4. Effects of Hsp70/Hsc70 on hERG currents in HEK293 cells stably expressing hERG-FLAG. Representative current traces recorded from cells transfected with Hsp70 or Hsc70 or mock plasmid (none) **(A)**. The membrane potential was held at −50 mV, depolarized by 1-sec test pulses ranging from −40 to +40mV and then repolarized back to the holding potential for tail current measurement. Average current–voltage relationships of peak and tail currents are shown in **B** and **C**. Values represent means±SEM. Differences between the control and the group with Hsp70 or Hsc70 were tested statistically. *$P<0.05$, †$P<0.01$ vs none (n=17 to 19).

siRNA prolonged half-life of both mutants. However, the effects were more prominent in F805C mutant (76% increase) than in P596R (29% increase) (Figure 8B).

Because HS could decrease the association of Hsc70 with hERG, we examined effects of HS on the stability of WT and 10 kinds of mutant hERG in transfected HL-1 cells. On IBs, WThERG-FLAG gave 2 intense bands, whereas the mutant proteins gave only a faint 135-kDa band (Figure 8C). HS dramatically increased not only the levels of the mature form of WT but also those of mutant hERG, and again this effect of HS was more prominent in those mutant proteins with intracellular domain mutations than those mutant located in the pore-region.

Previous studies have shown that specific hERG mutants can be stabilized by incubating the cells at low temperature.[4] We examined whether expression of hERG and its association with Hsp70 and Hsc70 were affected by hypothermia. WThERG-FLAG, P596R-FLAG, F805C-FLAG, R752W-FLAG and G601S-FLAG were transfected into HEK293 cells, then the cells were cultured at 37°C for 24 hours then at 27°C for 24 hours. The hypothermia increased not only the levels of WT mature and immature forms but also the levels of 2 forms of mutants (Figure 8D). IP experiment showed that the hypothermia decreased the association of mutant hERG with Hsc70 but not with Hsp70, suggesting that both WT and

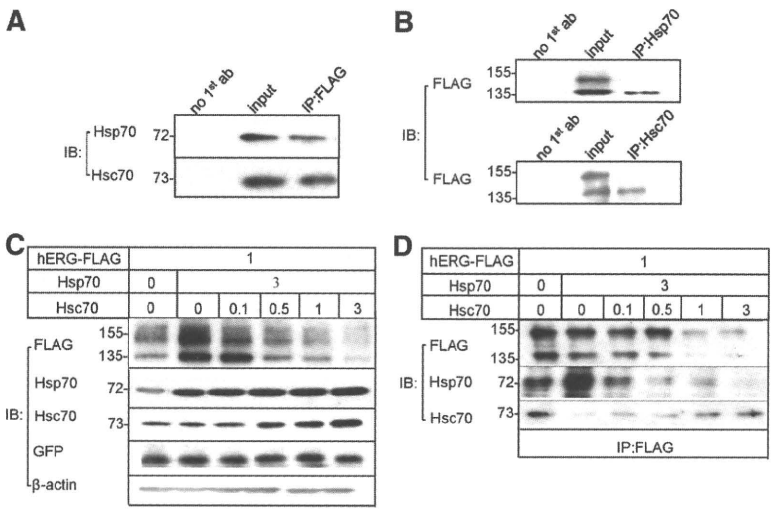

Figure 5. Effects of Hsc70 on Hsp70-induced increase of hERG-FLAG. A, Association of hERG-FLAG with Hsp70 or Hsc70. Anti-FLAG IPs from HEK293 cells transiently expressing hERG-FLAG were subjected to IB with anti-Hsp70 or Hsc70 antibody. No 1st ab represents a negative control with no primary antibody added and input is positive control. **B,** Anti-Hsp70 or Hsc70 IPs from HEK293 cells transiently expressing hERTG-FLAG were subjected to IB with anti-FLAG. **C,** HEK293 cells were transfected with indicated plasmids (μg). Whole-cell lysates were subjected to IB with indicated antibodies (n=4 to 6). **D,** Anti-FLAG IPs were subjected to IB with either anti-FLAG, Hsp70, or Hsc70 (n=6 to 7).

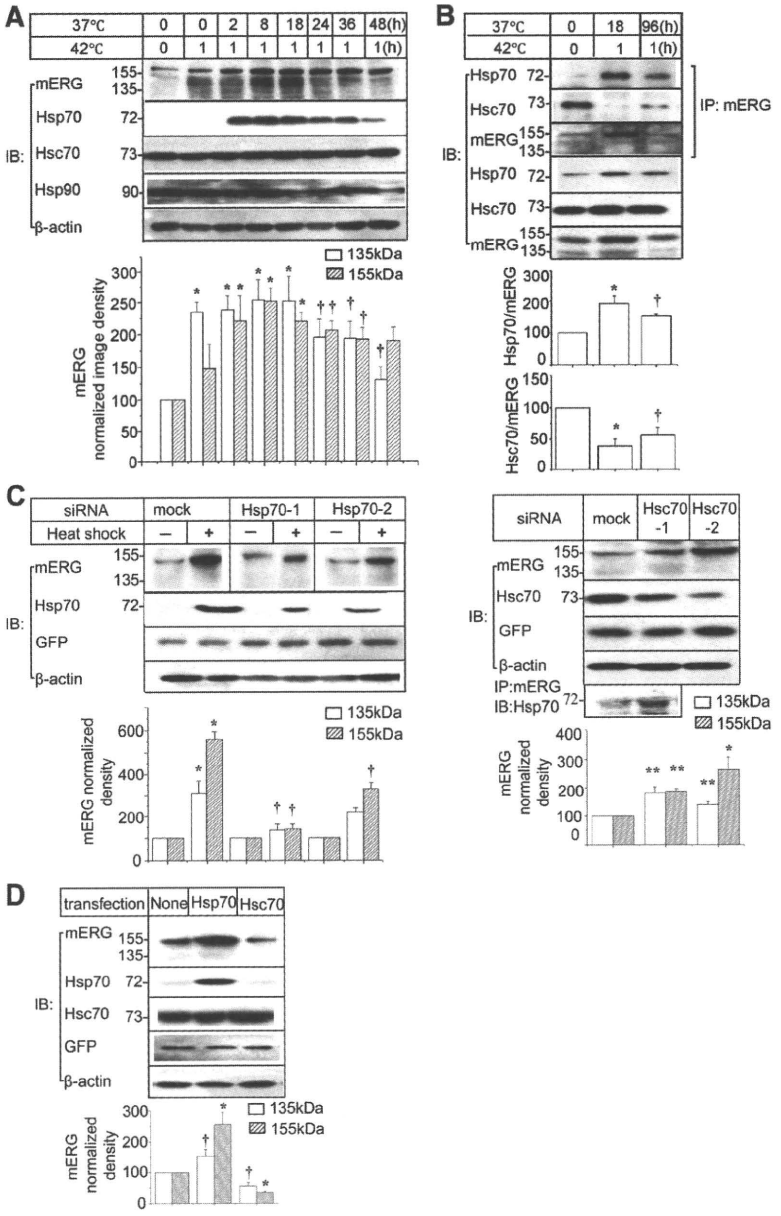

Figure 6. Effects of HS on the level of endogenous mouse ERG (mERG) in HL-1 cells. A, Cells were given a heat shocked at 42°C for 1 hour. The cells were recovered at the indicated times and analyzed by IB with indicated antibodies. Image densities of the immature and mature forms of mERG bands normalized to mERG expression levels in non-HS control cells (n=6 to 7, *$P<0.01$, †$P<0.05$ vs non-HS). **B,** Association of mERG with Hsp70 or Hsc70 was detected by IB. Anti-mERG IPs was subjected to IB. **Bar graphs** show the levels of Hsp70 or Hsc70 associated with mERG (n=4 to 5, *$P<0.01$, †$P<0.05$ vs non-HS group). **C**, HL-1 cells were transfected with a scramble siRNA (mock) or siRNAs against mouse Hsp70 **(left)** or Hsc70 **(right)**. The levels of mERG, Hsp70, and Hsc70 were analyzed by IB. Image density of mERG were quantified and normalized to mERG levels in the cells with a scramble siRNA (n=5 to 6, *$P>0.01$, **$P>0.05$ vs non-HS; †$P>0.05$ vs with a scramble siRNA with HS). **D,** Effects of Hsp70 or Hsc70 on endogenous mERG. HL-1 cells were transfected either with pcDNA3, Hsp70, or Hsc70 plasmid. Cell lysate was subjected to IB with the indicated antibodies (n=5 to 7, *$P<0.01$; †$P<0.05$ vs none).

mutant hERG proteins were stabilized because of disassociation from Hsc70 at low temperature.

Discussion

In the present study, we found that Hsp70 and Hsc70 exert opposite effects on the stability of hERG, ie, Hsp70 stabilized hERG, whereas Hsc70 destabilized it. The main site of action of these chaperones appeared to be the ER. Both Hsp70 and Hsc70 could associate with hERG and the stability control appeared to be a direct consequence of their association. We have also shown that the levels of these chaperones influenced cardiac APD. Evidence was also presented that disease-causing missense mutations of hERG alter its association with these chaperones.

Hsp70 and Hsc70 Exert Opposite Effects on the Stability of hERG

Hsp70 could be induced by HS and cellular stress, whereas Hsc70 is constitutively expressed.[23] These 2 proteins have a high degree of sequence homology and have been believed to be functionally interchangeable.[24–26] This is the first report to demonstrate that Hsp70 and Hsc70 exert opposite effects on the stability of hERG protein through their association with the immature form. In general, Hsp70 acts on nascent and newly synthesized proteins to hold them in a state competent for proper folding.[11] In contrast, Hsc70 associates with newly synthesized proteins to promote their proteasomal degradation. This effect of Hsc70 has been demonstrated for

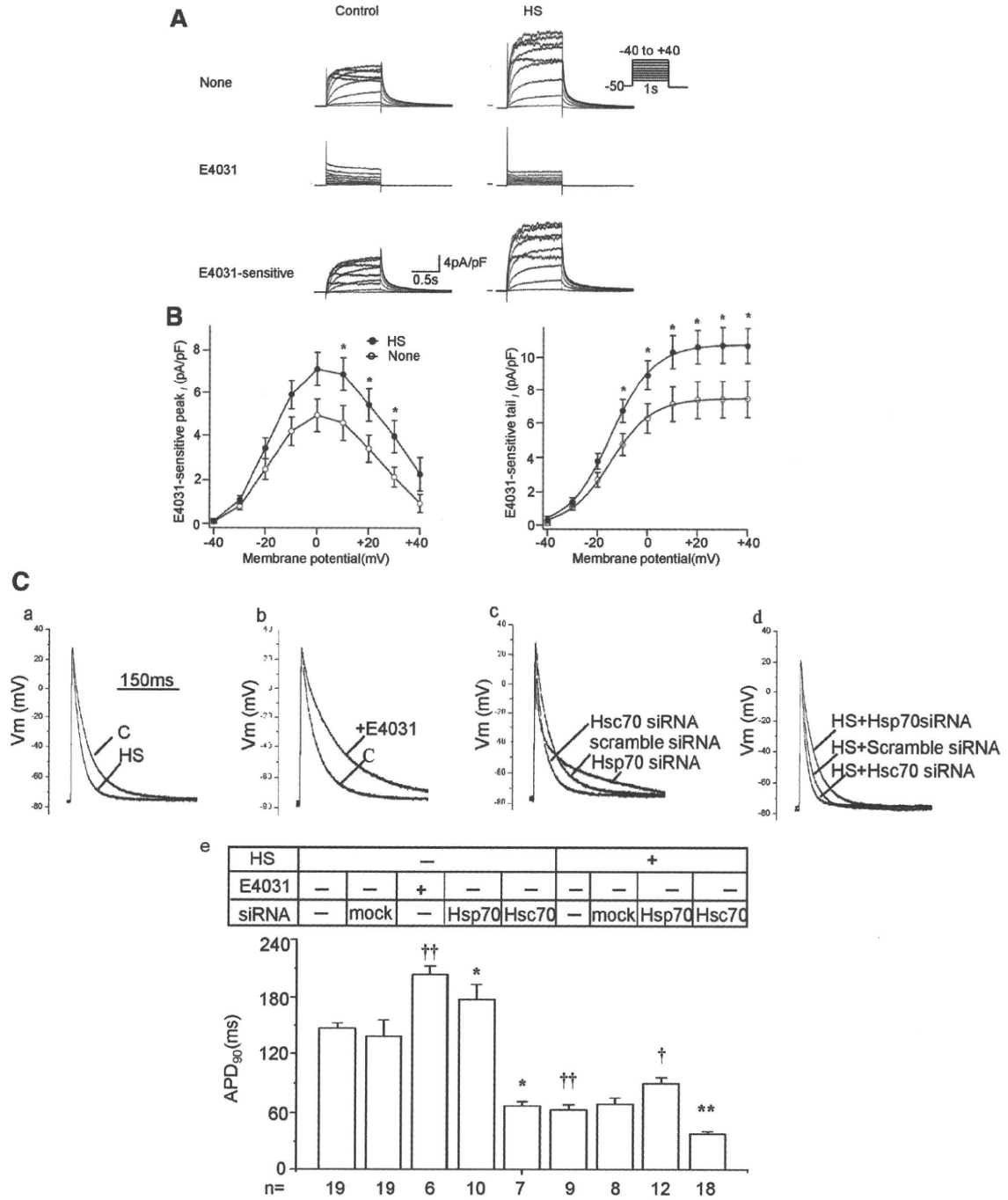

Figure 7. Effects of HS on E4031-sensitive currents and APD. A, Whole-cell membrane currents were recorded from a single HL-1 cell before (none) and after application of 10 μmol/L E4031. E4031-sensitive currents were obtained by digital subtraction. Current recordings were performed 24 hours after HS treatment at 42°C for 1 hour. **B,** Current–voltage relationships of the peak and tail of the E4031-sensitive currents (n=16, *$P<0.05$ vs none). **C,** Action potentials were recorded 24 hours after transfection of a scramble siRNA (mock) or a siRNA against Hsp70 or Hsc70 in the absence or presence of 10 μmol/L E4031. Representative action potentials are shown **(a through d)**. APD_{90} values are summarized as a bar graph **(e)**, and statistically evaluated: ††$P<0.01$ vs non-HS; *$P<0.01$ vs a scramble siRNA control non-HS; †$P<0.05$, **$P<0.01$ vs a scramble siRNA with HS treatment.

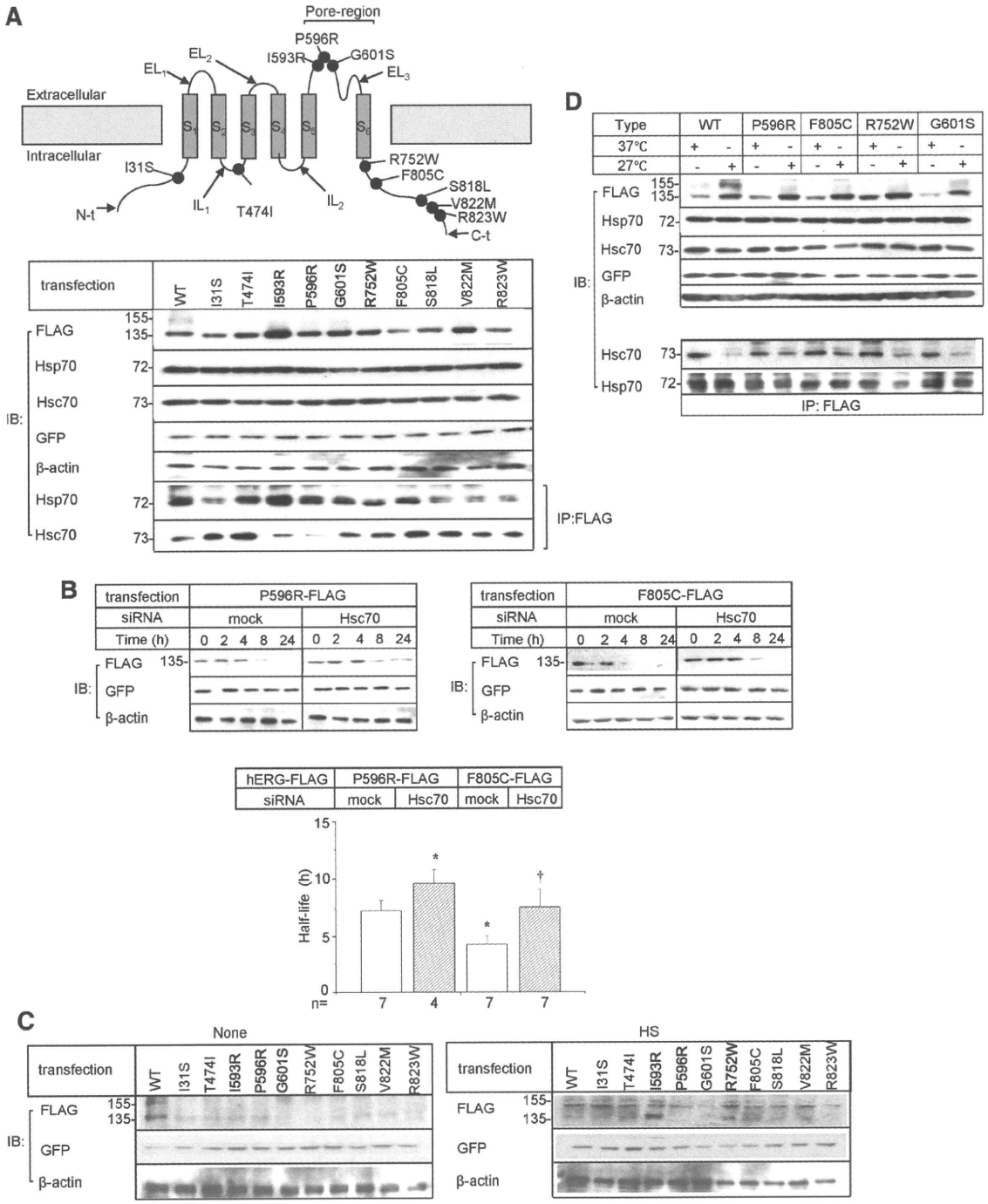

Figure 8. Effects of Hsp70 and Hsc70 on mutant hERG-FLAG. A, Top, Locations of LQT2-associated 10 mutations. **Black circles** indicate the locations of 10 missense mutations. The **arrows** point N terminus (N-t), intracellular loop (IL), extracellular loop (EL), and C terminus (C-t), respectively. WT hERG-FLAG and 10 kinds of mutant hERG-FLAG were transfected into HEK293 cells. Cell lysates or anti-FLAG IPs were subjected to IBs with indicated antibodies **(bottom). B,** Degradation of mutant hERG-FLAG. P596R-FLAG or F805C hERG-FLAG was transfected in HEK293 cells either with a scramble siRNA (mock) or an siRNA against Hsc70. Cells were chased for the indicated times after the addition of cycloheximide. Shown are representative Western blot with the indicated antibodies. Bar graphs summarize the half-life of 2 missense mutant hERG-FLAG. *$P<0.05$ vs P596R-FLAG with a scramble siRNA; †$P<0.05$ vs F805C-FLAG with a scramble siRNA. **C,** WT and mutant hERG-FLAG were transfected into HL-1 cell and the cells were given 1 hour of HS treatment at 42°C. Cell lysates were subjected to IB with indicated antibodies (n=4). **D,** Effects of hypothermia on WT and mutant hERG. Each construct was transfected into HEK293 cells. The cells were cultured at 37°C for 24 hours then at 27°C for 24 hours. The whole-cell lysates or anti-FLAG IPs were analyzed by IB with indicated antibodies (n=5 to 6).

CFTR,[27–29] murine epithelial sodium channel,[13] and $ASIC_2$ (acid-sensing ion channels).[30] Our findings are in agreement with those previous studies and presented evidence that Hsp/Hsc70 association with hERG is regulated by the cellular levels of these 2 chaperones (Figure 5C and 5D).

Hsp70/Hsc70 Controlled the Level of Endogenous mERG and the Cardiac APD

In this study, we identified that E4031-sensitive currents are the predominant component of the outward currents and show essentially the same characteristics as I_{Kr} in HL-1 murine cardiomyocytes. We demonstrated, for the first time, that HS was able to increase I_{Kr} and shorten cardiac APD. Under control conditions, Hsc70 associated with mERG to reduce the cellular level of mERG. HS- induced Hsp70 increases Hsp70-mERG complexes, causing an increase in the cellular level of mERG. The level of mERG is well known to regulate the activity of I_{Kr}[31] and I_{Kr} regulates cardiac APD, especially in mouse atrial myocytes,[19,32] which is one of the major factors to determine the QT interval.[22] E4031-induced prolongation of APD_{90} was more remarkable in the cells treated with HS than in the control cells, indicating that the increased I_{Kr} contributes to acceleration of repolarization by HS through increases in Hsp70-mERG complex associated with decreases of Hsc70-mERG complex. These data strongly suggest that Hsp70/Hsc70 plays a pivotal role in controlling APD in cells treated with HS. Our findings might explain fever-induced shortening of the QT interval.[33,34] Interestingly, siRNA knockdown of Hsc70 shortened APD in HL-1 cells, indicating that Hsc70 is able to regulate APD under physiological conditions. These results are in accordance with antiarrhythmic effects of augmented expression of hERG that have been reported in rabbit ventricular primary culture and a transgenic mice model.[35,36] In both cases, hERG expression resulted in significant shortening of APD and decreased the incidence of early afterdepolarizations.

Stability Control of hERG Mutant Proteins by Hsp70 and Hsc70

Most of LQT2 missense mutations decrease the stability of hERG.[4] This instability has been associated with increased association with Hsp70/ Hsc70, which have been suggested to play similar function.[8] We found that the association of Hsp70 and Hsc70 with mutant channels depended on the nature of the mutation. The level of Hsc70-F805C hERG complexes was higher than that of Hsc70–P596R hERG complexes resulting in a shorter half- life of F805C hERG proteins. The F805C mutant yielded smaller hERG currents than the P596R mutant.[4] Silencing Hsc70 prolonged the half-life of both mutant proteins but more predominantly in F805C, suggesting that Hsc70 determines degradation of their immature forms, especially those with the intracellular mutations.

Accordingly, HS promoted the maturation of mutant hERGs with mutations in intracellular domains rather than those in pore-region. It is conceivable that the HS-induced Hsp70 causes a disassociation of Hsc70 from mutant hERGs and increases the level of Hsp70-hERG complexes. hERG proteins contain a PAS (Per, Arnt, and Sim) domain on their N terminus and a cNBD domain on their C terminus; both of them may be targeted by cytosolic chaperones.[8] LQT2 mutations located in the N or C terminus might interfere the association of chaperones.[5] Ficker E et al reported decreased association of WT and mutant with Hsp70 /Hsc70 and increased hERG with reduced temperature.[8] We detected association of Hsp70 or Hsc70 with hERG separately and found that hypothermia decreased the level of Hsc70 associated with hERG, whereas it unaltered the level of Hsp70. Thus, the degradation of immature form of both WT and mutant hERG proteins was prevented by disassociation of Hsc70 under hypothermia. The biophysical characteristics of mutant hERG may be comparable with CFTRΔ508, a trafficking-deficient mutant. CFTRΔ508 can be rescued by Hsp70 and low-temperature culturing.[37,38] Both HS and low temperature result in disassociation of Hsc70 from mutant hERG proteins and stabilization of the immature form. Our data raise the possibility that Hsc70 and Hsp70 may be a target in the treatment of LQT2 which results from missense hERG mutations.

Acknowledgments

We acknowledge Dr William C. Claycomb (Louisiana State University) for the generous gift of HL-1 cells.

Sources of Funding

This work was supported by Ministry of Education, Culture, Sport, Science and Technology-Japan grant 21590931.

Disclosures

None.

References

1. Sanguinetti MC, Jiang C, Curran ME, Keating MT. A mechanistic link between an inherited and an acquired cardiac arrhythmia: HERG encodes the I_{Kr} potassium channel. *Cell*. 1995;81:299–307.
2. Sanguinetti MC, Tristani-Firouzi M. hERG potassium channels and cardiac arrhythmia. *Nature*. 2006;440:463–469.
3. Kiehn J, Lacerda AE, Wible B, Brown AM. Molecular physiology and pharmacology of HERG. Single-channel currents and block by dofetilide. *Circulation*. 1996;94:2572–2579.
4. Anderson CL, Delisle BP, Anson BD, Kilby JA, Will ML, Tester DJ, Gong Q, Zhou Z, Ackerman MJ, January CT. Most LQT2 mutations reduce Kv11.1 (hERG) current by a class 2 (trafficking-deficient) mechanisms. *Circulation*. 2006;113:365–373.
5. Thomas D, Kiehn J, Katus HA, Karle CA. Defective protein trafficking in hERG-associated hereditary long QT syndrome (LQT2): molecular mechanisms and restoration of intracellular protein processing. *Cardiovasc Res*. 2003;60:235–241.
6. Gong Q, Keeney DR, Molinari M, Zhou Z. Degradation of trafficking-defective long QT syndrome type II mutant channels by the ubiquitin-proteasome pathway. *J Biol Chem*. 2005;280:19419–19425.
7. Gong Q, Anderson CL, January CT, Zhou Z. Role of glycosylation in cell surface expression and stability of HERG potassium channels. *Am J Physiol Heart Circ Physiol*. 2002;283:H77–H84.
8. Ficker E, Dennis AT, Wang L, Brown AM. Role of the cytosolic chaperones Hsp70 and Hsp90 in maturation of the cardiac potassium channel HERG. *Circ Res*. 2003;92:87–100.
9. Petrecca K, Atanasiu R, Akhavan A, Shrier A. N-linked glycosylation sites determine HERG channel surface membrane expression. *J Physiol*. 1999;515:41–48.
10. Jakob U, Gaestel M, Engel K, Buchner J. Small heat shock proteins are molecular chaperones. *J Biol Chem*. 1993;268:1517–1520.
11. Hartl FU, Hayer-Hartl M. Molecular chaperones in the cytosol: from nascent chain to folded protein. *Science*. 2002;295:1852–1858.
12. Walker VE, Atanasiu R, Lam H, Shrier A. Co-chaperone FKBP38 promotes HERG trafficking. *J Biol Chem*. 2007;282:23509–23516.
13. Goldfarb SB, Kashlan OB, Watkins JN, Suaud L, Yan W, Kleyman TR, Rubenstein RC. Differential effects of Hsc70 and Hsp70 on the intracellular trafficking and functional expression of epithelial sodium channels. *Proc Natl Acad Sci U S A*. 2006;103:5817–5822.

14. Kato M, Ogura K, Miake J, Sasaki N, Taniguchi S, Igawa O, Yoshida A, Hoshikawa Y, Murata M, Nanba E, Kurata Y, Kawata Y, Ninomiya H, Morisaki T, Kitakaze M, Hisatome I. Evidence for proteasomal degradation of Kv1.5 channel protein. *Biochem Biophys Res Commun.* 2005;337:343–348.
15. Tanaka H, Miake J, Notsu T, Sonyama K, Sasaki N, Iitsuka K, Kato M, Taniguchi S, Igawa O, Yoshida A, Shigemasa C, Hoshikawa Y, Kurata Y, Kuniyasu A, Nakayama H, Inagaki N, Nanba E, Shiota G, Morisaki T, Ninomiya H, Kitakaze M, Hisatome I. Proteasomal degradation of Kir6.2 channel protein and its inhibition by a Na+ channel blocker aprindine. *Biochem Biophys Res Commun.* 2005;331:1001–1006.
16. Hirota Y, Kurata Y, Kato M, Notsu T, Koshida S, Inoue T, Kawata Y, Miake J, Bahrudin U, Li P, Hoshikawa Y, Yamamoto Y, Igawa O, Shirayoshi Y, Nakai A, Ninomiya H, Higaki K, Hiraoka M, Hisatome I. Functional stabilization of Kv1.5 protein by Hsp70 in mammalian cell lines. *Biochem Biophys Res Commun.* 2008;372:469–474.
17. Koshida S, Kurata Y, Notsu T, Hirota Y, Kuang TY, Li P, Bahrudin U, Harada S, Miake J, Yamamoto Y, Hoshikawa Y, Igawa O, Higaki K, Soma M, Yoshida A, Ninomiya H, Shiota G, Shirayoshi Y, Hisatome I. Stabilizing effects of eicosapentaenoic acid on Kv1.5 channel protein expressed in mammalian cells. *Eur J Pharmacol.* 2009;604:93–102.
18. Claycomb WC, Lanson NA Jr, Stallworth BS, Egeland DB, Delcarpio JB, Bahinski A, Izzo NJ Jr. HL-1 cells: a cardiac muscle cell line that contracts and retains phenotypic characteristics of the adult cardiomyocyte. *Proc Natl Acad Sci U S A.* 1998;95:2979–2984.
19. Toyoda F, Ding WG, Zankov DP, Omatsu-Kanbe M, Isono T, Horie M, Matsuura H. Characterization of the rapidly activating delayed rectifier potassium current, I (Kr), in HL-1 mouse atrial myocytes. *J Membr Biol.* 2010;235:73–87.
20. Xia M, Salata JJ, Figueroa DJ, Lawlor AM, Liang HA, Liu Y, Connolly TM. Functional expression of L- and T-type Ca2+ channels in murine HL-1 cells. *J Mol Cell Cardiol.* 2004;36:111–119.
21. Sartiani L, Bochet P, Cerbai E, Mugelli A, Fischmeister R. Functional expression of the hyperpolarization-activated, non-selective cation current I(f) in immortalized HL-1 cardiomyocytes. *J Physiol.* 2002;545:81–92.
22. Tan HL, Hou CJ, Lauer MR, Sung RJ. Electrophysiologic mechanisms of the long QT interval syndromes and torsade de pointes. *Ann Intern Med.* 1995;122:701–714.
23. Cvoro A, Korac A, Matic G. Intracellular localization of constitutive and inducible heat shock protein 70 in rat liver after in vivo heat stress. *Mol Cell Biochem.* 2004;265:27–35.
24. Takayama S, Xie Z, Reed JC. An evolutionarily conserved family of Hsp70/Hsc70 molecular chaperone regulators. *J Biol Chem.* 1999;274:781–786.
25. Brown CR, Martin RL, Hansen WJ, Beckmann RP, Welch WJ. The constitutive and stress inducible forms of hsp 70 exhibit functional similarities and interact with one another in an ATP-dependent fashion. *J Cell Biol.* 1993;120:1101–1112.
26. Freeman BC, Morimoto RI. The human cytosolic molecular chaperones hsp90, hsp70 (hsc70) and hdj-1 have distinct roles in recognition of a non-native protein and protein refolding. *EMBO J.* 1996;15:2969–2979.
27. Meacham GC, Patterson C, Zhang W, Younger JM, Cyr DM. The Hsc70 co-chaperone CHIP targets immature CFTR for proteasomal degradation. *Nat Cell Biol.* 2001;3:100–105.
28. Zhang H, Peters KW, Sun F, Marino CR, Lang J, Burgoyne RD, Frizzell RA. Cysteine string protein interacts with and modulates the maturation of the cystic fibrosis transmembrane conductance regulator. *J Biol Chem.* 2002;277:28948–28958.
29. Younger JM, Ren HY, Chen L, Fan CY, Fields A, Patterson C, Cyr DM. A foldable CFTR {Delta} F508 biogenic intermediate accumulates upon inhibition of the Hsc70-CHIP E3 ubiquitin ligase. *J Cell Biol.* 2004;167:1075–1085.
30. Vila-Carriles WH, Zhou ZH, Bubien JK, Fuller CM, Benos DJ. Participation of the chaperone Hsc70 in the trafficking and functional expression of ASIC2 in glioma cells. *J Biol Chem.* 2007;282:34381–34391.
31. Guo J, Massaeli H, Xu J, Jia Z, Wigle JT, Mesaeli N, Zhang S. Extracellular K+ concentration controls cell surface density of I_{Kr} in rabbit hearts and of the HERG channel in human cell lines. *J Clin Invest.* 2009;119:2745–2757.
32. Nakamura H, Ding WG, Sanada M, Maeda K, Kawai H, Maegawa H, Matsuura H. Presence and functional role of the rapidly activating delayed rectifier K^+ current in left and right atria of adult mice. *Eur J Pharmacol.* 2010;649:14–22.
33. Karjalainen J, Viitasalo M. Fever and cardiac rhythm. *Arch Intern Med.* 1986;146:1169–1171.
34. Amin AS, Herfst LJ, Delisle BP, Klemens CA, Rook MB, Bezzina CR, underkofler HA, Holzem KM, Ruijter JM, Tan HL, January CT, Wilde AA. Fever-induced QTc prolongation and ventricular arrhythmias in individuals with type 2 congenital long QT syndrome. *J Clin Invest.* 2008;118:2552–2561.
35. Nuss HB, Marban E, Johns DC. Overexpression of a human potassium channel suppresses cardiac hyperexcitability in rabbit ventricular myocytes. *J Clin Invest.* 1999;103:889–896.
36. Royer A, Demolombe S, Harchi AE, Le Quang K, Piron J, Toumaniantz G, Mazurais D, Bellocq C, Lande G, Terrenoire C, Motoike HK, Chevallier JC, Loussouarn G, Clancy CE, Escande D, Charpentier F. Expression of human ERG K^+ channels in the mouse heart exerts anti-arrhythmic activity. *Cardiovasc Res.* 2005;65:128–137.
37. Choo-Kang LR, Zeitlin PL. Induction of HSP70 promotes DeltaF508 CFTR trafficking. *Am J Physiol Lung Cell Mol Physiol.* 2001;281:58–68.
38. Collawn JF, Bebok Z, Matalon. Search and rescue: finding ways to correct deltaF508 CFTR. *Am J Respir Cell Mol Biol.* 2009;40:385–387.

Novelty and Significance

What Is Known?

- The human ether-a-gogo-related gene (hERG) encodes the potassium channel α-subunit, I_{Kr}, and its hereditary dysfunction causes long QT syndrome type 2 (LQT2).
- Heat shock protein (Hsp)70 stabilizes hERG protein to increase I_{Kr}.
- Heat shock cognate (Hsc)70, because of its high degree of sequence homology to Hsp70, may also influence hERG protein.

What New Information Does This Article Contribute?

- We found that Hsc70 destabilizes hERG proteins to decrease I_{Kr}, indicating that Hsc70 and Hsp70 reciprocally control the maturation of hERG proteins. Hsp70 competes with Hsc70 in the binding with hERG and facilitates its maturation.
- Heat shock–induced Hsp70 increases the level of the mature form of missense mutant hERG causing LQT2.

The hERG channel plays an important role in cardiac electric activity. It has been shown that inherited mutations in hERG or pharmacological block of I_{Kr} increases the risk of lethal arrhythmia. Here, we show for the first time that Hsc70 and Hsp70 exert reciprocal effects on stability of hERG proteins. We also found that maturation of disease-causing missense mutant hERGs could be restored by a heat shock. Similar effect was achieved by Hsc70 knockdown through a suppression of Hsc70-degradation pathway. Our study provides a new insight into pathogenesis of inherited arrhythmia at the molecular and cellular levels and may lead to a novel therapeutic approach for treating arrhythmias.

Circulation Journal
Official Journal of the Japanese Circulation Society
http://www.j-circ.or.jp

ORIGINAL ARTICLE
Arrhythmia/Electrophysiology

Atrioventricular Block-Induced Torsades de Pointes With Clinical and Molecular Backgrounds Similar to Congenital Long QT Syndrome

Yuko Oka, MD; Hideki Itoh, MD, PhD; Wei-Guang Ding, MD, PhD; Wataru Shimizu, MD, PhD; Takeru Makiyama, MD, PhD; Seiko Ohno, MD, PhD; Yukiko Nishio, MD; Tomoko Sakaguchi, MD, PhD; Akashi Miyamoto, MD; Mihoko Kawamura, MD; Hiroshi Matsuura, MD, PhD; Minoru Horie, MD, PhD

Background: Atrioventricular block (AVB) sometimes complicates QT prolongation and torsades de pointes (TdP).

Methods and Results: The clinical and genetic background of 14 AVB patients (57±21 years, 13 females) who developed QT prolongation and TdP was analyzed. Electrophysiological characteristics of mutations were analyzed using heterologous expression in Chinese hamster ovary cells, together with computer simulation models. Every patient received a pacemaker or implantable cardioverter defibrillator; 3 patients had recurrence of TdP during follow-up because of pacing failure. Among the ECG parameters, QTc interval was prolonged to 561±76 ms in the presence of AVB, but shortened to 495±42 ms in the absence of AVB. Genetic screening for *KCNQ1*, *KCNH2*, *SCN5A*, *KCNE1*, and *KCNE2* revealed four heterozygous missense mutations of *KCNQ1* or *KCNH2* in 4 patients (28.6%). Functional analyses showed that all mutations had loss of functions and various gating dysfunctions of I_{Ks} or I_{Kr}. Finally, action potential simulation based on the Luo-Rudy model demonstrated that most mutant channels induced bradycardia-related early afterdepolarizations.

Conclusions: Incidental AVB, as a trigger of TdP, can manifest as clinical phenotypes of long QT syndrome (LQTS), and that some patients with AVB-induced TdP share a genetic background with those with congenital LQTS. (*Circ J* 2010; **74:** 2562–2571)

Key Words: Atrioventricular block; Ion channels; Long QT syndrome; Torsades de pointes

The acquired form of long QT syndrome (LQTS) is a major cause of torsades de pointes (TdP),[1,2] which results from various factors, including drugs, bradycardia or hypokalemia. Regarding bradycardia, Kurita et al demonstrated that patients with bradycardia-induced TdP display abnormally prolonged QT intervals at slower heart rates (<60 beats/min) than those without TdP.[3] Some groups have reported the genetic background of bradycardia-induced TdP, as well as of congenital LQTS. In 2001, we reported a female with 2:1 atrioventricular block (AVB) and TdP, in whom the *KCNH2* A490T mutant was identified as heterozygous.[4] Subsequently, Lupoglazoff et al demonstrated that, in neonates, LQTS with 2:1 AVB is associated with *KCNH2* mutations whereas sinus bradycardia-related LQTS is associated with *KCNQ1* mutations.[5] Chevalier et al reported that among 29 patients with complete AVB and a QT interval >600 ms, 5 (17%) had mutations on genes encoding K^+ channels, and the expression test of these mutations showed functional changes compared with the wild-type (WT) K^+ current.[6]

Editorial p 2546

In Japan, some papers on congenital LQTS have been published,[2,7–9] but the molecular pathogenesis of AVB-related TdP has not been fully examined, particularly with respect to the relationship between genotype and cellular electrophysiology. The aim of this study was to investigate gene mutations and clarify their functional outcome in con-

Received May 31, 2010; revised manuscript received July 30, 2010; accepted August 2, 2010; released online October 21, 2010 Time for primary review: 16 days

Department of Respiratory and Cardiovascular Medicine (Y.O., H.I., T.S., A.M., M.K., M.H.), Department of Physiology (W.-G.D., H.M.), Shiga University of Medical Science, Otsu; Division of Cardiology, Division of Arrhythmia and Electrophysiology, Department of Cardiovascular Medicine, National Cerebral and Cardiovascular Center, Suita (W.S.); and Department of Cardiovascular Medicine, Kyoto University Graduate School of Medicine, Kyoto (T.M., S.O., Y.N.), Japan

Mailing address: Minoru Horie, MD, PhD, Department of Respiratory and Cardiovascular Medicine, Shiga University of Medical Science, Seta Tsukinowa-cho, Otsu 520-2192, Japan. E-mail: horie@belle.shiga-med.ac.jp

ISSN-1346-9843 doi:10.1253/circj.CJ-10-0498

secutive AVB patients complicated with TdP.

Methods

Study Population

The study cohort contained 14 consecutive probands, from unrelated families, who showed a prolonged QT interval and TdP associated with AVB. They were referred to 3 institutes in Japan; Shiga University of Medical Science (Otsu), National Cardiovascular Center (Suita), and Kyoto University Graduate School of Medicine (Kyoto) for LQTS genetic testing between 1996 and 2008.

Clinical Characterization

In each case, we recorded 12-lead electrocardiograms (ECGs) before and after AVB episodes, as well as gathering the results from other cardiovascular examinations and detailed clinical evaluations. Prolonged QT interval was diagnosed by the presence of prolongation of ventricular repolarization (corrected QT interval [QTc] >460 ms in lead V_5, according to Bazett's formula).[10] We excluded cases of TdP caused by AVB with drugs associated with QT prolongation, as well as those with active ischemia detected by noninvasive or invasive tests, including coronary angiography. We also investigated cardiac events in all 14 probands and their family members. Cardiac events were syncope, TdP, ventricular fibrillation (VF), aborted cardiac arrest (requiring defibrillation) or sudden cardiac death. We also followed the therapies and clinical prognoses of these patients.

Genetic Analysis

Genomic DNA was isolated from venous blood by QIAamp DNA blood midikit (Qiagen, Hilden, Germany). Established primer settings were used to amplify the entire coding regions of the known LQTS genes (*KCNQ1*, *KCNH2*, *SCN5A*, *KCNE1*, and *KCNE2*). Denaturing high-performance liquid chromatography (WAVE system Model 3500, Transgenomic, Omaha, NE, USA) was performed as described elsewhere, and abnormal conformers were amplified by polymerase chain reaction (PCR), and sequenced with an ABI PRISM-3130 sequencer (Perkin-Elmer Applied Biosystems, Wellesley, MA, USA). If we detected mutations in these genes, family members associated with the probands were also genetically analyzed. Formal informed consent was obtained from each patient or their guardians according to standards approved by local institutional review boards.

Expression Plasmids

The expression plasmids, pIRES2-EGFP/*KCNQ1*(wild-type; WT/*KCNQ1*) and pRc-CMV/*KCNH2* (WT/*KCNH2*) were kindly provided by Dr Barhanin (Université de Nice, Sophia Antipolis, Valbonne, France) and Dr Sanguinetti (University of Utah, Salt Lake City, UT, USA), respectively. The mutations were introduced using overlap PCR. The mutant plasmids were constructed by substituting the 838-bp *Xho*I-*Bgl*II for the G272V mutant, 464-bp *Hin*dIII-*Bst*XI for the D111V mutant, 1458-bp *Bst*XI-*Bgl*II for the A490T mutant, or 592-bp *Fse*I-*Sbf*I fragments for the P846T mutant for the corresponding fragments of WT/*KCNQ1* or WT/*KCNH2*. The nucleotide sequence of the construct was confirmed prior to the expression studies.

Expression in Chinese Hamster Ovary (CHO) Cells

CHO cells were maintained in Dulbecco's modified Eagle's medium and Ham's F12 nutritional mixture (Gibco-BRL, Rockville, MD, USA) supplemented with 10% fetal bovine serum (Gibco-BRL) and antibiotics (100 U/ml penicillin and 100 μg/ml streptomycin) in a humidified incubator gassed with 5% CO_2 and 95% air at 37°C. CHO cells were transiently transfected using 1 μg of WT/*KCNQ1* or mutant/*KCNQ1*, and 1 μg of pIRES-CD8/*KCNE1* per 35-mm dish, using the LipofectAMINE method according to the manufacturer's instructions (Invitrogen, Carlsbad, CA, USA). In some experiments, 0.5 μg of WT/*KCNQ1* was transfected with or without mutant/*KCNQ1*, instead of 1 μg of WT/*KCNQ1*. Cells successfully transfected with both *KCNQ1* and *KCNE1* cDNA were selected by green fluorescent protein (GFP) and decoration with anti-CD8 antibody-coated beads (Dynabeads CD8; Dynal Biotech, Oslo, Norway). The cells were transiently transfected with either WT/*KCNH2* or mutant/*KCNH2*, using the LipofectAMINE method according to the manufacturer's instructions. For a 35-mm dish the amount of plasmid was 2 μg and 0.175 μg of GFP; only GFP-positive cells were used for the patch-clamp study.

Electrophysiological Experiments

Whole-cell patch-clamp recordings were conducted at 37.0±1.0°C using an EPC-8 patch-clamp amplifier (HEKA, Lambrecht, Germany) 48–72 h after transfection. No leak subtraction was used. The normal Tyrode solution contained (in mmol/L): NaCl 140, KCl 5.4, $CaCl_2$ 1.8, $MgCl_2$ 0.5, NaH_2PO_4 0.33, glucose 5.5, and HEPES 5 (pH adjusted to 7.4 with NaOH). The pipette solution contained (in mmol/L): potassium aspartate 70, KCl 40, KH_2PO_4 10, EGTA 5, $MgSO_4$ 1, Na_2-ATP (Sigma, St Louis, MO, USA) 3, Li_2-GTP 0.1, and HEPES 5 (pH adjusted to 7.4 with KOH). A coverslip with adherent CHO cells was placed on the bottom of a glass recording chamber (0.5 ml in volume) mounted on the stage of an inverted microscope (TE2000-U, Nikon, Tokyo, Japan). Pipette resistance was 3–5 MΩ when filled with internal solution. Currents and voltages were digitized and voltage commands were generated through an LIH-1600 AD/DA interface (HEKA) controlled by PatchMaster software (HEKA). Current amplitude was divided by membrane capacitance (Cm) to obtain current densities (pA/pF) in each cell. The voltage-dependence of current activation was determined by fitting the normalized tail current (I_{tail}) vs test potential (V_{test}) to a Boltzmann function:

$$I_{tail} = 1/(1+\exp[(V_{0.5}-V_t)/k]),$$

where $V_{0.5}$ indicates the voltage at which the current is half-maximally activated and k is the slope factor.

Computer Simulation of Action Potential Duration (APD)

Ventricular action potentials were simulated by using the dynamic Luo-Rudy model with recent modifications.[11,12] The ratio of I_{Kr} and I_{Ks} conductance was set at 23:1, 17:1, and 19:1 in the epicardium, endocardium, and M cell layer, respectively. Based on the experimental data of voltage-clamp recordings of *KCNH2* channels heterologously expressed in CHO cells, we constructed Markov or Hodgkin-Huxley models for simulated mutant channels as compared with mutants associated with congenital LQTS. In order to construct mutant channel models, we decreased the conductance of each channel as appropriate for the decreased current density, and looked for adequate changes in mutant channels by changing each coefficient value, in turn, for gating states associated with impaired gating defects. The simulation for voltage-clamp experiments was calculated using the 4th-order Runge-Kutta method with a fixed-time step of

Table 1. Clinical Characteristics and Gene Mutations of Probands With Bradycardia-Induced Torsades de Pointes

Case no.	Age (years)	Sex (M/F)	Diagnosis	Cardiac events	Family history	ECG at AVB		ECG without AVB		Therapy	Follow-up		Mutation/Gene
						QTc (ms)	HR (beats/min)	QTc (ms)	HR (beats/min)		Period (months)	Arrhythmic events	
1	27	F	2:1 AVB	TdP	–	600	50	545	71	PM	41	None	A490T/KCNH2
2	74	F	CAVB	TdP	–	NA	NA	NA	NA	PM	22	None	
3	73	M	CAVB	TdP	–	635	39	NA	NA	PM	104	None	
4	57	F	CAVB	TdP	–	525	43	545	61	ICD, BB, Ib	96	None	D111V/KCNH2
5	69	F	2:1 AVB	TdP	–	452	45	476	86	PM, BB, Ib	84	None	
6	21	F	Wenckebach AVB	TdP	Sudden death	625	65	489	75	ICD, Ib	79	VF because of Wenckebach AVB	
7	76	F	2:1 AVB	TdP	–	578	50	424	83	PM, BB	59	None	G272V/KCNQ1
8	71	F	CAVB	TdP	–	729	57	489	72	ICD	46	None	P846T/KCNH2
9	73	F	CAVB	TdP	–	567	33	NA	NA	PM	129	None	
10	62	F	CAVB	TdP	–	473	29	NA	NA	PM	277	None	
11	68	F	CAVB	TdP	–	552	39	NA	NA	PM	207	TdP because of V pacing failure	
12	38	F	CAVB	TdP	Mother with LQTS	493	28	500	65	PM, BB	NA	NA	
13	76	F	CAVB	TdP	–	500	46	NA	NA	PM	57	TdP because of low back-up rate	
14	18	F	CAVB	TdP	–	570	47	NA	NA	PM	130	None	
Ave±SD	57±21					561±76	44±11	495±42	64±27		102±71		

AVB, atrioventricular block; TdP, torsades de pointes; PM, pacemaker; CAVB, complete atrioventricular block; NA, not available; ICD, implantable cardioverter defibrillator; BB, β-blocker; Ib, class Ib antiarrhythmic drugs; VF, ventricular fibrillation.

0.02 ms. The simulation programs were coded in C++ and implemented for personal computers.[12]

Statistical Analysis

Numerical data are presented as mean±standard error of the mean. Student's t-test was used to compare the data between different groups for electrophysiological measurement, and differences were considered significant at $P<0.05$.

Results

Clinical Characteristics of the Patients in This Study

The clinical characteristics of the 14 patients enrolled in the study are presented in **Table 1**. The mean age at the onset of AVB was 57±21 years, and 13 patients (92.8%) were females. All patients showed TdP with AVB: 10 had complete AVB, 3 had 2:1 AVB, and 1 had Wenckebach AVB. No patient had experienced syncope or ventricular arrhythmias prior to the appearance of TdP. One patient (case 6 in **Table 1**) with Wenckebach AVB had 2 family members who had suddenly died at the age of 1 year and 3 months, respectively. The mother of case 12 (**Table 1**) had atrial fibrillation, mitral regurgitation, and complete AVB with prolonged QT interval, but no TdP.

In most patients with AVB-related TdP, the tachyarrhythmia started from premature ventricular contractions after a long-pause interval following ventricular arrhythmias, so-called "TdP from short–long–short pattern" (**Figure 1D**).[13] The ECGs available at the time of AVB showed severely prolonged QT interval (heart rate 44±11 beats/min and QTc 561±76 ms). On the other hand, the ECGs without AVB available in 7 cases also showed a prolonged QT interval (heart rate 64±27 beats/min, $P<0.05$, and QTc 495±42 ms, P=NS, vs those in AVB). ECGs in sinus rhythm were obtained in 4 and 3 patients before and after AVB, respectively.

All patients underwent implantation of either an implantable cardioverter-defibrillator (ICD) or permanent pacemaker (PM), together with the administration of several drugs, including β-blockers (ICD n=3; PM n=11). Mean clinical follow-up during advanced therapy was 102±71 months. After the placement of a PM or ICD, 2 patients maintained own ventricular beats but the other 12 depended on ventricular pacing during the follow-up period. Three patients had recurrence of TdP even while receiving treatment. Patient no. 11 suddenly experienced repetitive TdP because of pacing failure and no. 13 also experienced TdP when her own ventricular beats had been set faster than the basal pacing rate. In patient 6, the reappearance of Wenckebach AVB without ventricular pacing caused ventricular tachycardia. In all 3 cases, no gene mutations were detected.

Molecular Genetics and Clinical Characteristics of Patients With Gene Mutations

The genetic analysis revealed different heterozygous mutations in 4 (28.6%) of 14 AVB-related TdP cases (**Table 1**): 1 *KCNQ1* mutation, G272V, and 3 *KCNH2* mutations, D111V, A490T and P846T (**Figure 1A**). All were located in the nonpore regions; G272V is located in the S5 domain for the *KCNQ1* channel; D111V, A490T, and P846T are located in the N-terminus, S2–S3 inner loop, and C-terminal domains for the *KCNH2* channel, respectively (**Figure 1B**). In the remaining 10 patients, we were unable to detect any mutations associated with the 5 major LQTS-related genes.

G272V in *KCNQ1* (Case 7 in Table 1) The G272V muta-

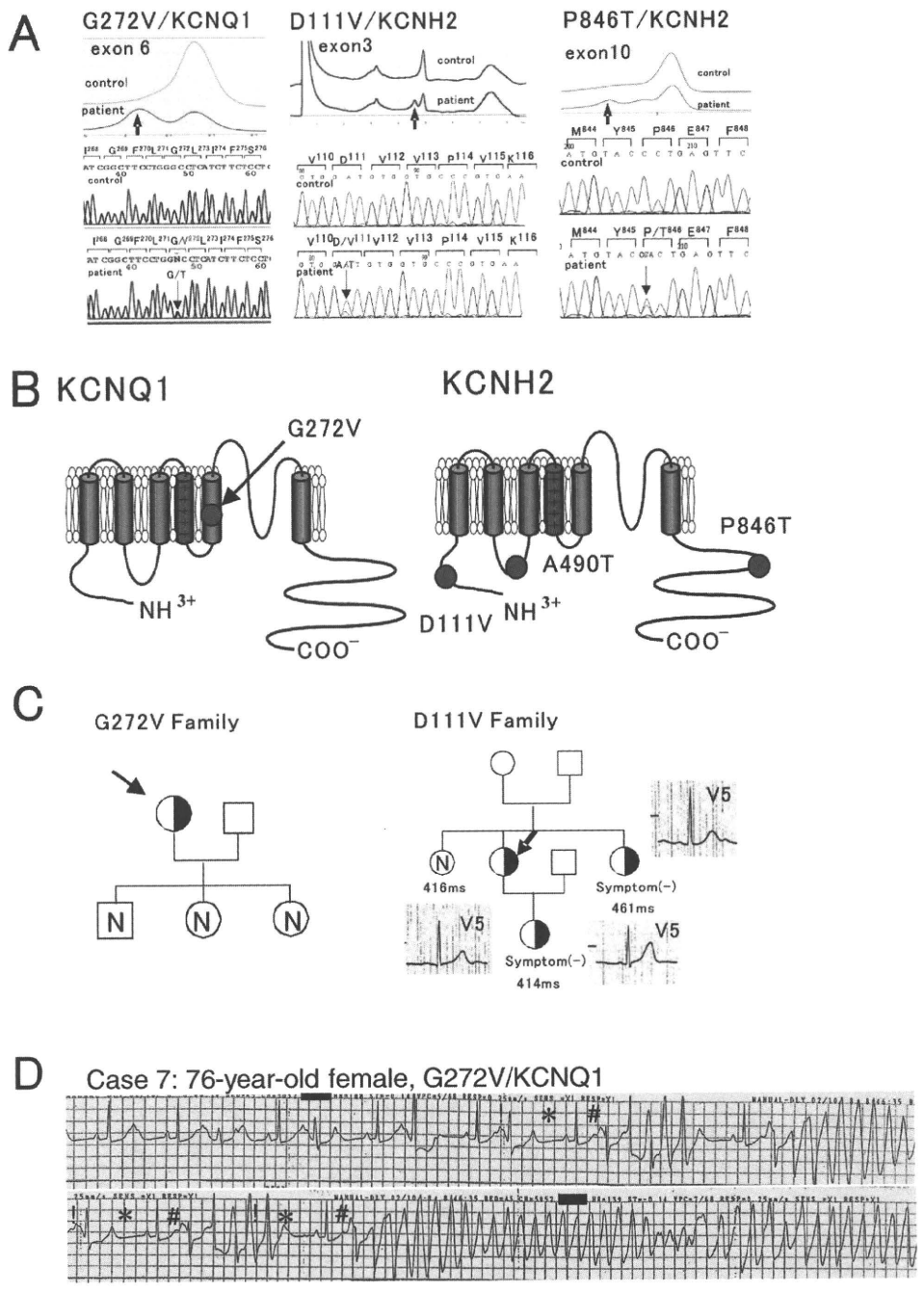

Figure 1. Molecular discovery and clinical data associated with *KCNQ1* and *KCNH2* mutations, and the initiation of atrioventricular block -related torsades de pointes (TdP). (**A**) Denaturing high-performance liquid chromatography patterns and DNA sequence data in normal controls and patients with G272V for *KCNQ1* (**Left**), D111V for *KCNH2* (**Middle**), and P846T for *KCNH2* (**Right**). (**B**) Schemes showing the topology of cardiac ion channel proteins for *KCNQ1* and *KCNH2* and the location of mutations identified in this study. (**C**) Two pedigrees of G272V and D111V families. Circles and squares represent female and male family members, respectively; probands are indicated by arrows. Heterozygous carriers are represented as half-filled symbols, family members in whom no genetic data were available are shown by open symbols, and non-carriers by open symbols with N. QTc intervals corrected by Bazzet's formula in lead V5 are given for each available family member. (**D**) Representative ECG recordings from case 7 (76-year-old female with G272V-KCNQ1 mutation). TdP during 2:1 AV block started with so-called "short (!)–long (*)–short (#) pattern" which resulted in a long pause (*).[13]

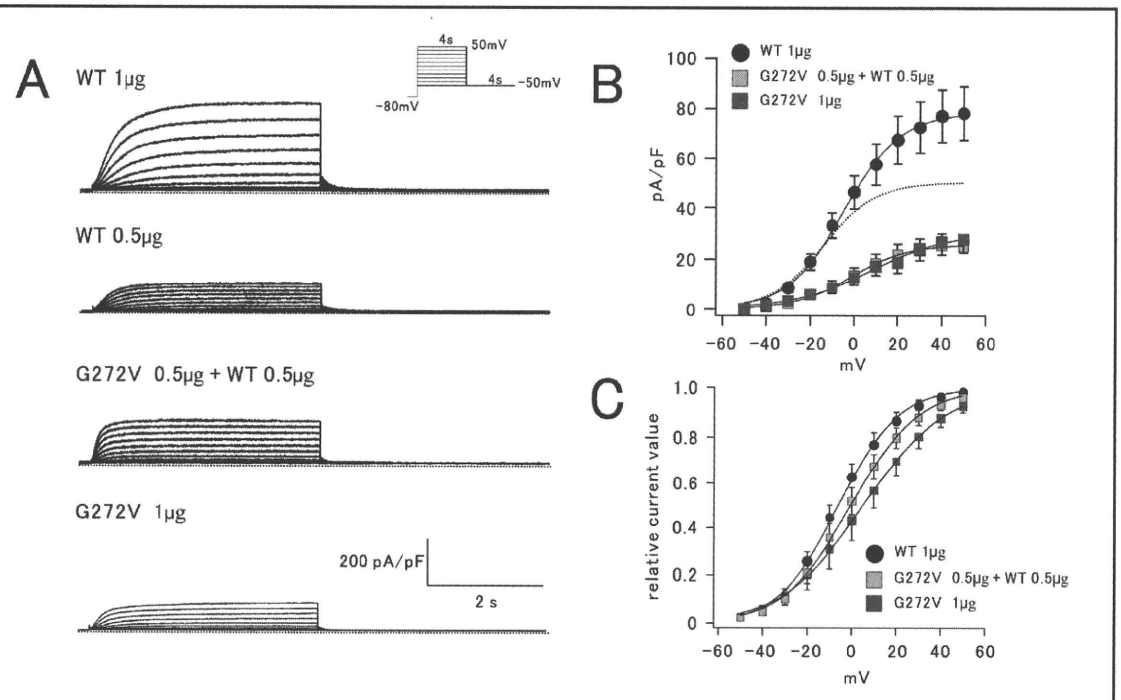

Figure 2. G272V KCNQ1 mutant channel shows loss of function associated with decreased density on I_{Ks}. Functional analyses on wild-type (WT) and G272V mutant channels expressed in Chinese Hamster ovary cells. (**A**) Representative current recordings for each channel. Currents were elicited from a holding potential of −80 mV, by depolarizing pulses (4-s duration) from −50 to +50 mV (with a 10-mV step increment) and subsequent repolarization to −50 mV for a 4-s duration (inset). Concentrations of cDNAs used for transfection are indicated near each graph. (**B**) Tail current-voltage relationships for 1 μg WT (closed circles; n=18), 0.5 μg WT (indicated by dotted line; n=14), 0.5 μg WT plus 0.5 μg G272V (green squares; n=19), 1 μg G272V (red squares; n=11). (**C**) Normalized activation curves by fitting to Boltzmann function.

tion was identified in a 76-year-old female who did not have a particularly relevant family history (**Figure 1A Left panel**). For approximately 10 years, she had taken nilvadipine and gliclazide because of hypertension and diabetes mellitus. Approximately 1 year before hospitalization, her QTc interval was within normal range (424 ms). When she was admitted to hospital because of syncope, her monitoring ECGs displayed 2:1 AVB (50 beats/min), prolonged QTc interval (578 ms), and repetitive TdP (**Figure 1D**). Her serum K^+ level was low (2.5 mEq/L). Because AVB persisted, she underwent DDD PM implantation. After correction of the serum K^+ level and PM therapy, her QTc interval shortened and TdP disappeared. She was free from cardiac events for the following 59 months. The genetic analysis revealed 3 children as non-mutation carriers (**Figure 1C Left panel**).

D111V in *KCNH2* (Case 4 in Table 1) The D111V mutation was identified in a 57-year-old female who did not have a particularly relevant family history (**Figure 1A Middle panel**). She experienced syncope after eating breakfast, and the monitoring ECG in the ambulance documented complete AVB (43 beats/min), prolonged QTc interval (525 ms) and TdP. After external PM therapy was initiated, TdP disappeared. She then underwent ICD implantation and started oral mexiletine hydrochloride (300 mg/day) and propranolol hydrochloride (30 mg/day); she has had no cardiac events over a follow-up period of 96 months. However, her QTc interval has remained prolonged even in the absence of AVB (545 ms, 4 years later). The genetic tests in her 3 relatives showed 2 mutation carriers (**Figure 1C Right panel**): a 51-year-old sister and 29-year-old daughter. Both these relatives were asymptomatic. Her daughter's QTc interval was within normal range (414 ms), but the sister's was prolonged (461 ms).

P846T in *KCNH2* (Case 8 in Table 1) The P846T mutation was found in a 71-year-old female who did not have a particularly relevant family history (**Figure 1A Right panel**). She experienced syncope after breakfast, and the monitoring ECG in the ambulance displayed complete AVB (45 beats/min) and repetitive TdP with prolonged QT interval. On admission, her AV conduction resumed at 57 beats/min, but her QTc interval remained prolonged (729 ms). After ICD implantation, she was free from cardiac events for 46 months, but her QTc interval remained prolonged (489 ms). We did not conduct a genetic analysis in this family.

A490T in *KCNH2* (Case 1 in Table 1) We have previously reported the clinical features of a A490T mutation identified in a 27-year-old female.[3] Briefly, her 12-lead ECG showed severe bradycardia because of 2:1 AVB (50 beats/min) with complete left bundle branch block and remarkable prolongation of QTc interval (600 ms). She fainted and collapsed while talking on the telephone, and the Holter ECG showed TdP associated with 2:1 AVB.

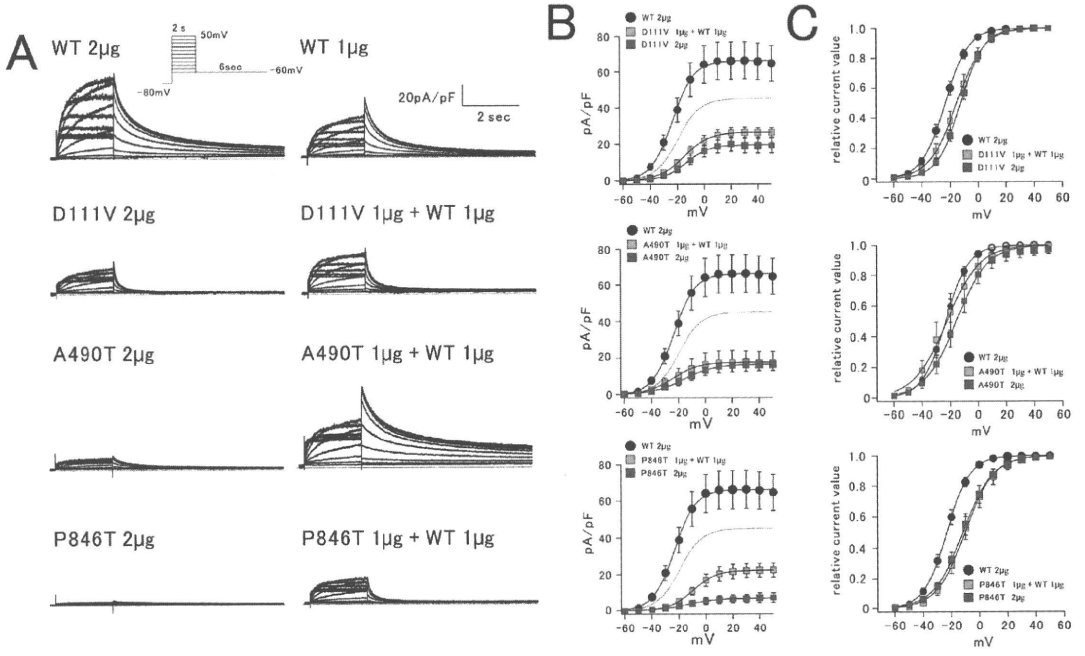

Figure 3. All *KCNH2* mutant channels show loss of function associated with decreased density on I_{Kr}. Electrophysiological characteristics of *KCNH2* mutant channels in Chinese Hamster ovary cells. (**A**) Families of representative current traces. Experimental protocol is shown in the inset. Concentrations of cDNAs used for transfection are indicated above each graph. (**B**) Tail current-voltage relationships for 2 μg wild-type (WT: closed circles; n=20), 1 μg WT (dotted line; n=14), 1 μg WT plus 1 μg mutant (green squares; n=10–13), 2 μg mutant (red squares; n=8–12). (**C**) Normalized activation curves by fitting to Boltzmann function.

Table 2. Parameters of Inactivation in WT and Mutant *KCNH2*

	WT (n=16)	WT/D111V (n=16)	D111V (n=15)	WT/A490T (n=17)	A490T (n=15)	WT/P846T (n=15)	P846T (n=16)
$V_{0.5}$ (mV)	−58.3±4.7	−40.1±4.1**	−47.4±7.0	−32.5±3.9*	−44.2±3.3	−38.7±2.4**	−55.5±3.5
Slope factor	29.2±1.4	33.9±1.3	35.3±1.7**	30.6±1.4†	34.9±1.1**	33.0±0.6†	37.5±1.7*

*P<0.001 vs WT, **P<0.01 vs WT, †P<0.05 vs WT.
WT, wild-type.

Expression Study

In order to clarify the functional consequences of the G272V mutation of *KCNQ1* and the D111V, A490T, and P846T mutations of *KCNH2*, we assessed the electrophysiological properties of the WT and mutant clones by using CHO cells.

Biophysical Assay of *KCNQ1* Mutant Channel Figure 2A shows representative examples of whole-cell currents recorded from CHO cells transfected with WT/*KCNQ1*, G272V/*KCNQ1* alone or WT co-expressed G272V/*KCNQ1* (WT/G272V) plus *KCNE1*. CHO cells transfected with WT/*KCNQ1* (1 or 0.5 μg) displayed outward currents with slow activation/deactivation kinetics on depolarization, which are typical of I_{Ks} currents, as previously reported.[14,15] In contrast, a cell transfected with G272V/*KCNQ1* (1 μg) displayed smaller I_{Ks} currents compared with that of the WT (1 μg). WT/G272V at an equimolar ratio (0.5 μg) also showed smaller I_{Ks} currents.

In Figure 2B, the tail current densities at −50 mV measured in multiple cells are plotted as a function of test pulse voltages (between −50 and +50 mV). The tail current densities at −50 mV after depolarizing test pulses to +40 mV were 77.0±11 pA/pF for 1 μg WT (n=18), 49.5±7.9 pA/pF for 0.5 μg WT (n=14), 25.4±4.5 pA/pF for 0.5 μg WT/G272V (n=19) (vs WT 1 μg, P<0.001), 26.7±4.9 pA/pF for 1 μg G272V (n=11) (vs WT 1 μg, P<0.01). Thus, compared with the WT I_{Ks} current, co-transfection of the mutant affected the expressed current densities.

Figure 2C represents the voltage-dependence of current activation. Tail current densities after each test potential were fitted to a Boltzmann function (see Methods). The parameters were $V_{0.5}$=−5.2±3.0 mV, k=11.1±0.6 for 1 μg WT, $V_{0.5}$=−1.0±3.7 mV, k=11.7±1.1 for 0.5 μg WT/G272V, $V_{0.5}$=5.7±5.4 mV, k=14.3±1.6 (vs WT 1 μg; P<0.05) for 1 μg G272V. Regarding half-activation voltages, WT plus G272V and G272V tended to shift to the depolarization side compared with WT but there was no statistical significance. In

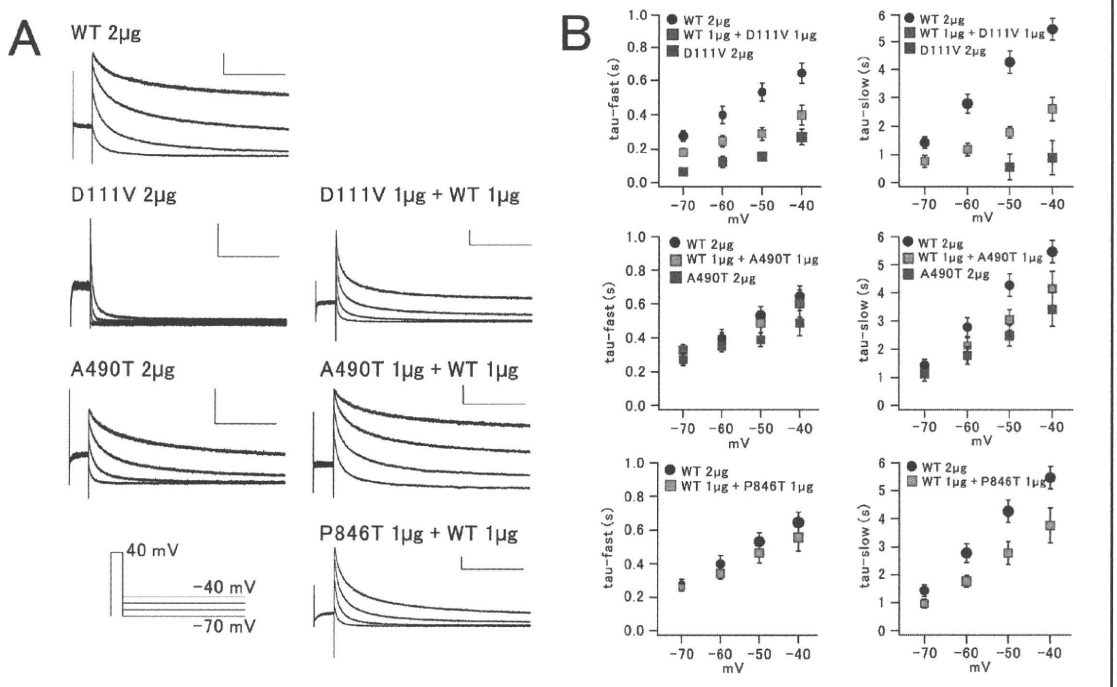

Figure 4. *KCNH2* mutant channels show a faster deactivation. (**A**) Representative tail currents elicited after depolarization to +40 mV (inset protocol). (**B**) Deactivation process was fitted to 2 components having different time constants, tau-fast and tau-slow. They were calculated in a pooled data from multiple cells transfected by 3 mutants (from top of panel B, D111V, A490T and P846T, respectively) and are plotted against membrane potentials (–70 to –40), for 2 μg WT (closed circles; n=15), 1 μg WT plus 1 μg mutant (green squares; n=7–14 for each channel), 2 μg mutant (red squares; n=6–8).

slope factors, G272V alone channel was larger than WT ($P<0.05$). Overall, the most important finding was the dominant-negative effect for the G272V channel.

Biophysical Assay of 3 *KCNH2* Mutant Channels Figure 3A shows representative examples of whole-cell currents recorded from CHO cells transfected with WT/*KCNH2* (2 and 1 μg), mutant/*KCNH2* (2 μg), or WT co-expressed mutant/*KCNH2* (WT/mutant) (1 μg each). CHO cells transfected with WT/*KCNH2* (2 or 1 μg, **Figure 3A Upper 2 panels**) displayed outward currents with inward rectifying properties, which are typical of I_{Kr} currents.[16] In contrast, the magnitude of currents from cells expressing all of the WT/mutants and mutant only were remarkably reduced (**Figure 3A Lower 6 panels**).

In **Figure 3B**, the tail current densities at –60 mV are plotted as a function of test pulse voltages (between –60 and +50 mV). The mean current densities after depolarizing test pulse to +20 mV in WT channels were 66.2±11 pA/pF for 2 μg (n=20) and 45.0±9.3 pA/pF for 1 μg (n=14). In contrast, those in the WT/mutant and mutant channels were 25.1±2.9 pA/pF in WT/D111V (n=13), 15.8±6.0 pA/pF in WT/A490T (n=10), 20.5±3.9 pA/pF in WT/P846T (n=12), 18.8±3.6 pA/pF for D111V (n=9), 15.2±3.4 pA/pF for A490T (n=12), 6.1±2.3 pA/pF for P846T (n=8), respectively. They were all significantly smaller than those of the 2-μg WT channels (vs WT 2 μg; $P<0.01$). **Figure 3C** shows that all WT/mutant and mutant channels tended to shift to the depolarization side compared with the WT. Overall, all mutant channels showed loss of function associated with a dominant-negative effect and shift of the activation curve to depolarization.

We then examined whether the mutations affected the inactivation kinetics of mutant channels using a double-pulse protocol. $V_{0.5}$ and the slope factor of steady-state inactivation differed between WT and WT plus mutant or mutant. All mutant *KCNH2* channels showed the shift of inactivation curves to depolarizing direction, and the differences were statistically significant (**Table 2**). Therefore, we also changed the parameters associated with inactivation states in the following simulation study.

Figure 4A depicts original current traces showing deactivation at 4 different repolarization potentials (from –70 to –40 mV) of WT and/or mutant/*KCNH2*. Deactivating currents were best fit with a double-exponential function, and are summarized in **Figure 4B**. At 4 different potentials, both time constants (Tau-fast and Tau-slow) for D111V and WT/D111V were smaller than those of the WT. Tau-slow of WT/P846T was also smaller than those of the WT. We could not assess that of P846T (2 μg), because it was too small to measure. In contrast, there were no significant changes between the WT and WT/A490T or A490T in the deactivation process.

Computer Simulation of APD

In order to compare how functional changes caused by mutations affect ventricular action potentials, a simulation study

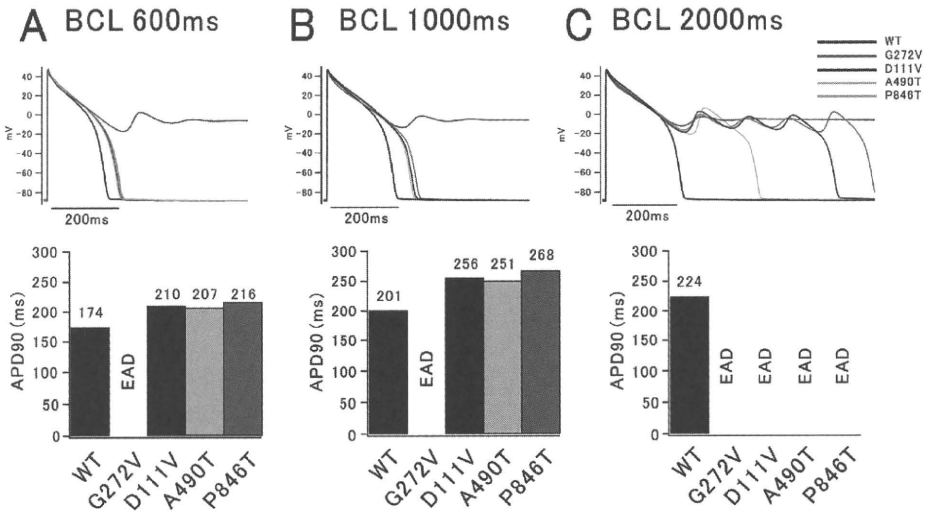

Figure 5. Computer simulations with Luo-Rudy myocardial model show bradycardia-induced early afterdepolarization (EAD). Each figure presents (**A**) action potential duration (APD) at basic cycle length (BCL) of 600 ms, (**B**) APD at BCL of 1,000 ms, and (**C**) APD at BCL of 2,000 ms. The longer the BCL in each model was, the more the APD was prolonged. EADs appeared in the models of D111V/WT, A490T/WT, and P846T/WT only at BCL of 2,000 ms, but appeared at all BCLs in the case of G272V/WT.

Table 3. Parameters of Simulation Data in Bradycardia-Induced Long QT Syndrome

Gene	Mutation	WT basal parameters	Mutant changed parameters
KCNQ1	G272V	gsk=0.202*(1+0.6/(1+pow(0.000038/cai),1.4)))	gsk=0.067*(1+0.6/(1+pow(0.000038/cai),1.4)))
		xs1 ss=1/(1+exp(-(v-1.5)/16.7))	xs1 ss=1/(1+exp(-(v-6.5)/16.7))
KCNH2	D111V	gherg=0.0135*pow(Kout,0.59)	gherg=0.331*0.0135pow(Kout,0.59)
		$\alpha\alpha$=65.5e-3*exp(0.05547153*(v-36))	$\alpha\alpha$=65.5e-3*exp(0.05547153*(v-69))
		αi=0.439*exp(–0.02352*(v+25))*4.5/Kout	αi=0.439*exp(–0.02352*(v+3))*4.5/Kout
		$\beta\beta$=2.9375e-3*exp(–0.02158*v)	$\beta\beta$=2*2.9375e-3*exp(–0.02158*v)
KCNH2	A490T	gherg=0.0135*pow(Kout,0.59)	gherg=0.1887*0.0135pow(Kout,0.59)
		αi=0.439*exp(–0.02352*(v+25))*4.5/Kout	αi=0.439*exp(–0.02352*(v-6))*4.5/Kout
KCNH2	P846T	gherg=0.0135*pow(Kout,0.59)	gherg=0.265*0.0135pow(Kout,0.59)
		$\alpha\alpha$=65.5e-3*exp(0.05547153*(v-36))	$\alpha\alpha$=65.5e-3*exp(0.05547153*(v-80))
		αi=0.439*exp(–0.02352*(v+25))*4.5/Kout	αi=0.439*exp(–0.02352*(v+3))*4.5/Kout
		$\beta\beta$=2.9375e-3*exp(–0.02158*v)	$\beta\beta$=1.3*2.9375e-3*exp(–0.02158*v)

was conducted using the Luo-Rudy model, which incorporated the Markov[13] or Hodgkin-Huxley[17] process gating for the mutant channels (**Figure 5**). **Table 3** shows the parameters of simulation that were changed to fit to experimental results. We simulated action potentials in all myocardial layers at 3 different basic cycle lengths (BCL 600, 1,000, 2,000 ms) (**Figures 5A–C**). In the endocardium and epicardium, APD of all mutant models was prolonged, but did not produce early afterdepolarizations (EAD) (data not shown in **Figure 5**). In contrast, in the simulated M cell layer, APD was lengthened significantly at a slower heart rate. In the lower half of **Figure 5**, below each simulated action potential, the corresponding bar graphs show APDs at 90% repolarization. Three APD models with D111V, A490T, and P846T displayed EADs at BCL of 2,000 ms, whereas G272V displayed it at all BCLs.

Discussion

There are 3 major findings in the present study. (1) In 4 of 14 consecutive AVB-associated TdP patients, 3 *KCNH2* and 1 *KCNQ1* heterozygous missense mutations were identified. (2) Electrophysiological analyses revealed loss of function associated with decreased current densities and various dysfunctions on I_{Ks} or I_{Kr} in 4 mutants. (3) Functional changes reconstituted by the computer simulation resulted in a prolonged APD and EAD under condition of bradycardia.

During AVB, our 14 patients showed a prolonged QT interval and TdP. Based on a comparison of ECGs available before and after AVB, we found the QT intervals were lengthened even in the absence of AVB. These clinical characteristics indicate that AVB-related TdP might share a similar genetic background with congenital LQTS: mutations on cardiac ion channel genes could be partially causative. Lupo-